Research Square

Preprints are preliminary reports that have not undergone peer review.
They should not be considered conclusive, used to inform clinical practice,
or referenced by the media as validated information.

Mineralogical, Physicochemical, and Geochemical Characterization of Swelling Clay-Rich Materials and Estimation of Sodium Carbonate Requirements for Activation: A Comparative Approach

Hanane AIT HMEID

h.aithmeid@ump.ac.ma

Chouaib Doukkali University

Aboubakr LIDALT

Mohamed First University

Said ADARDOR

Mohammed VI Polytechnic University, Morocco University

Mustapha AKODAD

Mohamed First University

Ghizlane HAMDIOUI

Mohamed First University

Mouhssin EL HALIM

Cadi Ayyad University

Chaouki SADIK

Hassan II University of Casablanca

Abdelilah MIHRAJE

Chouaib Doukkali University

Khalid EL KHALIDI

Chouaib Doukkali University

Anas SALHI

Chouaib Doukkali University

Ibrahim DAKIR

Chouaib Doukkali University

Research Article

Keywords: Bentonite, Smectite, Sodium activation, Sodium carbonate dosage, Cation exchange capacity, Divalent cations

Posted Date: November 19th, 2026

DOI: https://doi.org/10.21203/rs.3.rs-11528007/v1

License: This work is licensed under a Creative Commons Attribution 4.0 International License.
Read Full License

Additional Declarations: No competing interests reported.

Mineralogical, Physicochemical, and Geochemical Characterization of Swelling Clay-Rich Materials and Estimation of Sodium Carbonate Requirements for Activation: A Comparative Approach

Hanane AIT HMEID[1,*], Aboubakr LIDALT[2,*], Said ADARDOR[3], Mustapha AKODAD[2], Ghizlane HAMDIOUI[2], Mouhssin EL HALIM[4], Chaouki SADIK[5], Abdelilah MIHRAJE[1], Khalid EL KHALIDI[1], Anas SALHI[6], Ibrahim DAKIR[1].

[1] Marine Geosciences and Soil Sciences Laboratory, Department of Geology, Faculty of Sciences, Chouaib Doukkali University, El Jadida24000, Morocco

[2] Laboratory OLMAN-BPGE, Multidisciplinary Faculty of Nador, Mohamed First University, Oujda, Morocco

[3] Geology and Sustainable Mining, Mohammed VI Polytechnic University, Benguerir 43150, Morocco University, El Jadida 24000, Morocco

[4] Laboratoire de Géosciences et Environnement, Faculty of Sciences and Techniques, Cadi Ayyad University, BP 549 Marrakech, Morocco

[5] Laboratory of Physical Chemistry of Applied Materials (LCPMA). Geomaterials, Energy Efficiency and Environment Team (G3E), Faculty of Sciences Ben M'Sick, Hassan II University of Casablanca, Casablanca, Morocco

[6] Laboratory of Water and Environment department of Chemistry, Faculty of Sciences, Chouaïb Doukkali University

*Correspondence: h.aithmeid@ump.ac.ma; aithmeid.hanane@ucd.ac.ma https://orcid.org/0000-0002-4941-4373

Abstract

This study investigates bentonite geomaterials collected from the eastern part of Jbel Tidiennt, one of the satellite volcanic edifices of the Gourougou Massif, in the Neogene Kert Basin, northeastern Morocco. It aims to characterize their mineralogical, physicochemical, and geochemical properties and to estimate the sodium carbonate (Na_2CO_3) requirements for sodium activation. The raw geomaterials were characterized using particle-size analysis, physicochemical measurements, X-ray diffraction (XRD), Fourier-transform infrared spectroscopy (FTIR), thermal analysis, cation exchange capacity (CEC) determination, and major- and trace-element analyses. The results revealed a predominantly smectitic composition, with smectite contents ranging from 58 to nearly 89 wt.%, alkaline pH values (8.2–9.0), and relatively high CEC values, although significant variations in cation composition were observed among the samples.

Two complementary approaches were used to estimate the theoretical Na_2CO_3 dosage, addressing the two main objectives of sodium activation: increasing Na^+ saturation of the exchange complex to promote

cation exchange, smectite particle exfoliation, swelling, and dispersion, and promoting the precipitation of divalent Ca^{2+} and Mg^{2+} ions as carbonates to limit their potential interference with clay mineral behavior. The first approach was based on CEC and the initial exchangeable sodium content, with a target activation degree of 110%. The second approach considered the total soluble and exchangeable Ca^{2+} and Mg^{2+} contents to estimate the Na_2CO_3 requirement for their potential precipitation as carbonates. The calculated dosages ranged from 2.5 to 4.2 wt.% for the CEC-based approach and from 2.6 to 4.3 wt.% for the divalent-cation-based approach. The differences between these estimates highlight the influence of the chemical parameters used to calculate the activation requirements. For each sample, selecting the higher dosage obtained from the two approaches provides a conservative preliminary estimate for subsequent activation trials. The results contribute to the assessment of sodium activation requirements for Moroccan bentonite geomaterials and provide a basis for further experimental investigation of their activation behavior and potential industrial applications.

Keywords: Bentonite; Smectite; Mineralogical and geochemical characterization; Sodium activation; Sodium carbonate dosage; Cation exchange capacity; Divalent cations.

I- Introduction

Clay minerals represent a major group of naturally occurring geomaterials owing to their abundance in the Earth's crust and their wide range of physicochemical properties (Aboudi Mana et al. 2017 ; Kumari and Mohan 2021 ; El Farricha 2022). Their high adsorption capacity, cation-exchange ability, water-retention potential, and reactive surface characteristics make them essential materials in a variety of natural processes and industrial applications (Randhawa, 2024). Among clay minerals, bentonites are of particular interest due to their unique properties, which provide significant technological, environmental, and economic advantages.

Bentonite was originally known as ‘mineral soap’ or ‘soap clay (Hosterman and Patterson 1992 ; Sutherland 2024). It is a clay-rich rock composed predominantly of minerals belonging to the smectite group, particularly montmorillonite, which generally constitutes the dominant mineralogical phase (Murray 2006 ; Laine and Karttunen 2010 ; Belousov and Karelina 2022). It is formed through the natural or hydrothermal alteration of volcanic ash deposits rich in volcanic glass that accumulated in either marine or continental environments (Grim and Guven 1978 ; Huff 2016 ; Belousov and Karelina 2022). During their geological evolution, these pyroclastic materials undergo complex mineralogical transformations leading to the formation of clay minerals characterized by a layered structure and a high specific surface area

(Arslan et al. 2010). In addition to montmorillonite, bentonites may contain various accessory phases, including quartz, feldspars, calcite, and gypsum, as well as other clay minerals such as chlorite, vermiculite, illite, and kaolinite (Ross and Shannon 1926 ; Ait Hmeid et al. 2021a ; García-Rivas et al. 2025).

The properties of bentonites are closely related to their mineralogical composition and to the nature of the exchangeable cations present in the interlayer spaces of smectite minerals (Reid-Soukup and Ulery 2002). Montmorillonite, which is generally the predominant mineral phase in bentonites, is a 2:1 (TOT) phyllosilicate consisting of one octahedral sheet, mainly composed of Al and Mg, sandwiched between two tetrahedral silica sheets. Isomorphic substitutions within the tetrahedral and octahedral sheets generate a permanent negative layer charge, which is compensated by exchangeable interlayer cations, such as Na^{+}, Ca^{2+}, and Mg^{2+}, together with water molecules (Zhao et al. 2021) **(Figure 1)**. The nature and valence of these exchangeable cations strongly influence the hydration state, basal spacing, interlayer interactions, and swelling behavior of montmorillonite (Wilson et al. 2006 ; Yotsuji et al. 2021). In Na^{+}-dominated montmorillonite, the weaker electrostatic attraction between the negatively charged layers and the monovalent Na^{+} ions favors greater hydration and a larger interlayer distance, typically ranging from approximately 1.2 to 1.5 nm, resulting in a higher swelling capacity. In contrast, Ca^{2+}-dominated montmorillonite generally exhibits a smaller interlayer distance, typically around 0.95–1.0 nm, due to stronger electrostatic interactions between the divalent Ca^{2+} ions and the negatively charged layers. This stronger interlayer attraction limits hydration and swelling, resulting in a lower swelling capacity compared with Na^{+}-dominated montmorillonite (Li et al. 2024). Therefore, the type and valence of the exchangeable interlayer cations play a key role in controlling the structural, hydration, and swelling properties of montmorillonite.

Accordingly, bentonites are commonly classified according to their dominant exchangeable cation as sodium- or calcium-rich bentonites. Sodium bentonites generally exhibit high swelling capacity, strong dispersion in water, and favorable colloidal and rheological properties (Gilg et al. 2020). In contrast, calcium bentonites generally display lower swelling capacity but may exhibit significant adsorption and ion-exchange properties (Muhammad and Siddiqua 2022 ; Ait Hmeid et al. 2025). To improve their technological performance, calcium bentonites can be activated by treatment with sodium carbonate, which promotes the exchange of interlayer Ca^{2+}

by Na^+ and consequently enhances their swelling capacity, dispersion, and rheological properties (Charkaoui et al. 2025).

Owing to these remarkable properties, bentonites are widely used in numerous industrial sectors. They constitute a key component of drilling muds in the oil and gas industry, where they ensure wellbore stability, facilitate the transport of drill cuttings, and control fluid loss. They are also employed as binders in the foundry industry and as rheological additives in paints, inks, cosmetics, and various industrial fluids (Patel et al. 2006 ; Harvey and Lagaly 2013 ; Ebrahim et al. 2026). In addition, bentonites are extensively used in civil engineering and environmental applications for the construction of impermeable barriers, containment systems, and geotechnical structures (Di Emidio et al. 2017 ; Cao et al. 2021). Their use further extends to the agricultural sector, where they contribute to the improvement of the hydro-physical and chemical properties of soils.

Bentonite deposits are widely distributed throughout the world. The largest reserves of sodium bentonite are located in the western United States, particularly in the states of Wyoming, Montana, and South Dakota, which are considered global reference areas for highly swelling bentonites (Davis and Vacher 1940 ; Dixon et al. 1992 ; Sutherland 2024). Significant deposits are also exploited in Europe, Asia, Australia, South America, and Africa. In Morocco, bentonitic resources are mainly concentrated in the Nador region, within the Neogene basins of Kert and Melilla (El Miz et al. 2017 ; Ait Hmeid et al. 2020 ; Et-Tayea et al. 2023 ; Imame et al. 2025). These formations are associated with Neogene volcanism of the Gourougou massif and primarily result from the in situ alteration of volcanic glass-rich materials.

Among these deposits, the bentonites of the Neogene Kert Basin represent one of the most important clay resources in northeastern Morocco (Nasri et al. 2019 ; Belghazdis et al. 2022 ; Rachidi et al. 2024). Despite their economic and industrial significance, the spatial variability in mineralogical composition, exchangeable cation chemistry, and technological behavior of these bentonites remains insufficiently integrated into current valorization and industrial optimization approaches. This heterogeneity may significantly influence key parameters such as rheological properties, cation exchange capacity, and the efficiency of sodium carbonate activation treatments, which directly control their performance in industrial applications.

Furthermore, although the bentonites from the Nador region have attracted increasing interest, studies that comprehensively integrate mineralogical, geochemical, and technological aspects

remain relatively limited. In particular, the relationships between smectite content, exchangeable cation composition, the presence of soluble salts, and the efficiency of sodium activation have not yet been sufficiently documented. A better understanding of these parameters is essential for predicting the industrial behavior of bentonites and optimizing their utilization in applications requiring high swelling capacity and well-controlled rheological properties.

In the context of the growing demand for value-added clay materials, the characterization of Moroccan bentonites is essential for optimizing their industrial utilization. Advances in analytical techniques now enable the establishment of clear relationships between mineralogical composition, physicochemical properties, and technological performance.

Accordingly, the present study aims to evaluate the sodium activation potential of bentonites from Jbel Tidiennit (Nador, Morocco) by determining their theoretical sodium carbonate requirement based on cation exchange capacity (CEC) and exchangeable cation composition. This approach makes it possible to define the optimal activation conditions and to assess the influence of mineralogical characteristics on the technological behavior of bentonites after sodium activation treatment.

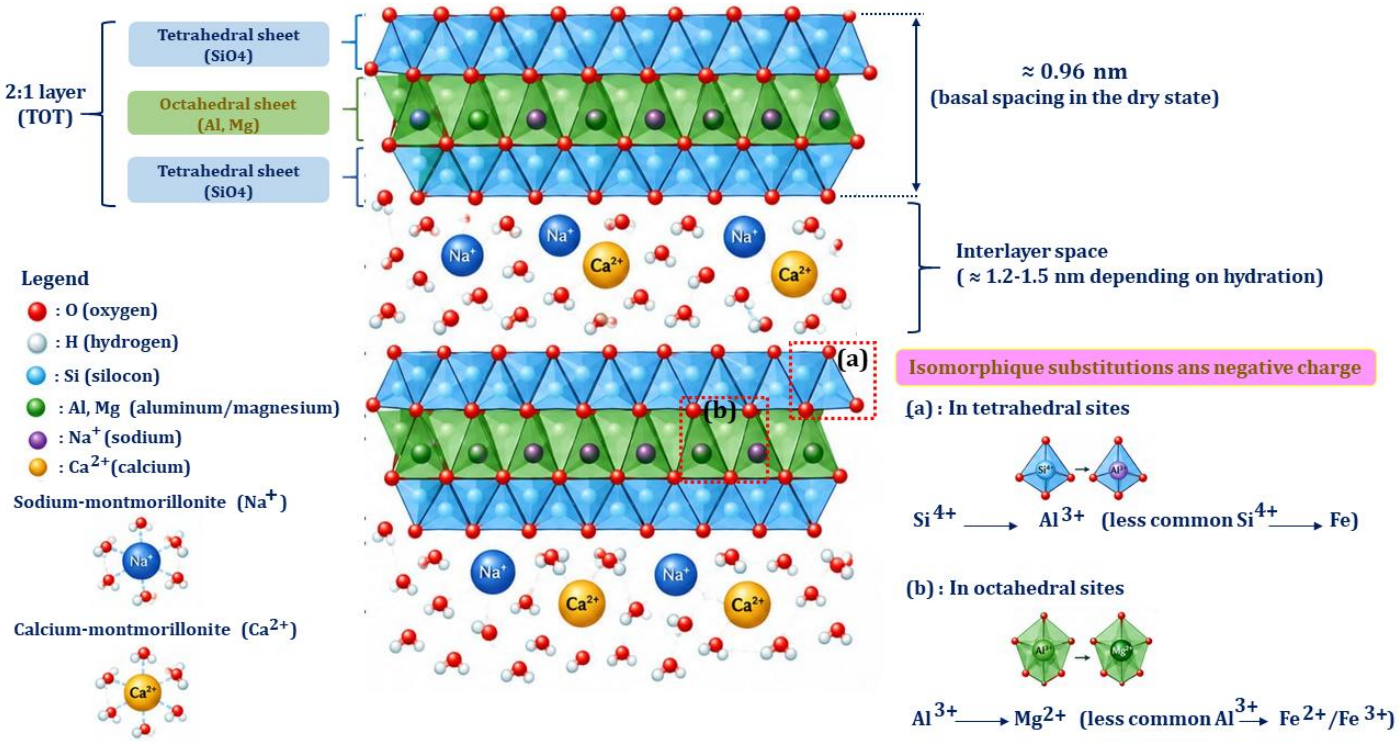


Figure 1. Schematic representation of the 2:1 (TOT) structure of montmorillonite.

II- Geological Setting

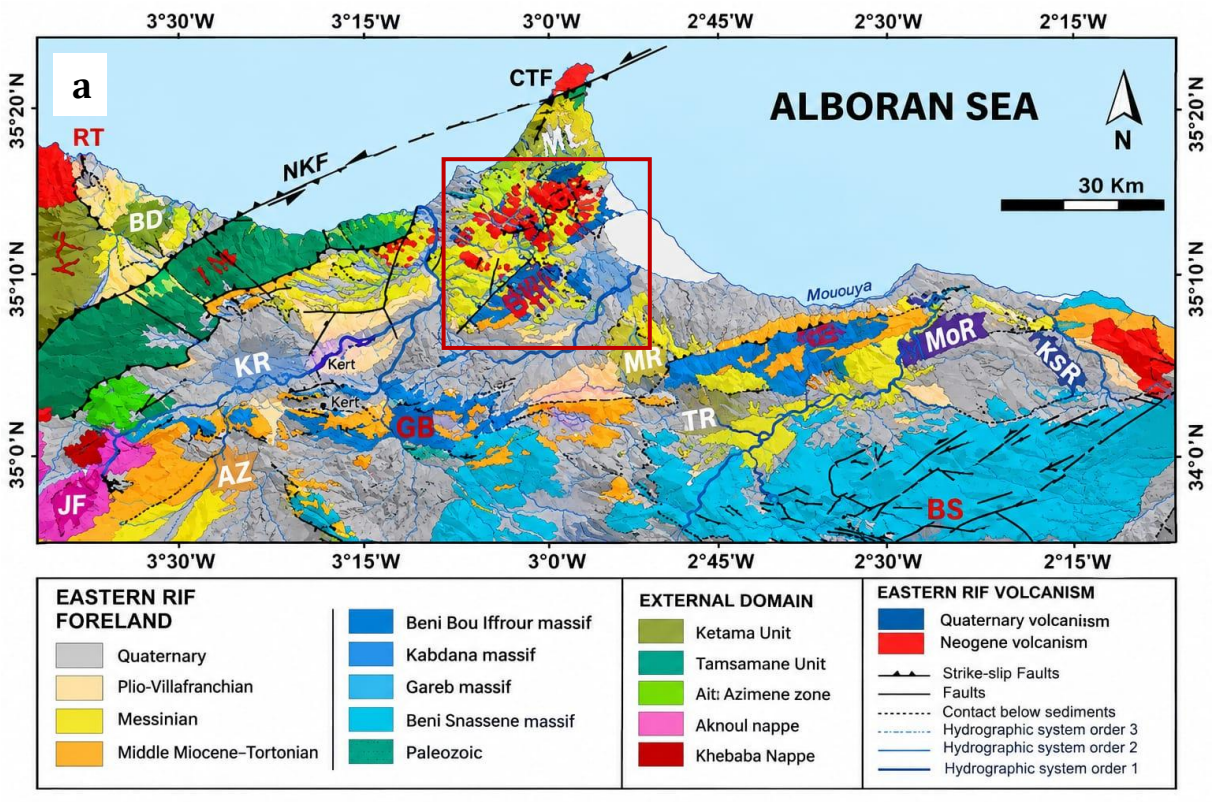
The studied bentonite deposit is located near Zeghanghane, within the municipality of Beni Sidel Louta, Nador Province, northeastern Morocco, in the Kert Basin of the Eastern Rif. The Kert Basin is a Neogene basin that developed in relation to the tectonic evolution of the Rif Alpine belt during the convergence between the African and Eurasian plates (Suter 1965 ; Leblanc 1979 ; Münch et al. 2001 ; Chalouan et al. 2006 ; Azdimousa et al. 2007 ; Barcos et al. 2014). Its structural evolution involved successive compressional, strike-slip, and extensional tectonic phases, which influenced basin subsidence, sedimentation, and volcanic activity (Michard et al. 2007 ; Martín-Martín et al. 2022). The basin contains a heterogeneous Miocene–Quaternary sedimentary and volcano-sedimentary succession, including marine and continental marls, reefal limestones, detrital deposits, pyroclastic materials, and volcanic rocks (Martín-Martín et al. 2020). Regional fault systems played an important role in controlling sedimentation and the emplacement of volcanic products **(Figure 2a)**.

The Neogene volcanic activity of the Nador region is closely associated with the Gourougou volcanic complex and several satellite volcanic centers, including the Tidiennit massif (Rachidi et al. 2024 ; Seidi et al. 2024). The Tidiennit volcanic massif, located approximately 18 km from Nador within the external domain of the Rif Chain (Louaya and Hamoumi 2010), consists predominantly of rhyolitic lava flows, pyroclastic deposits, volcanic breccias, volcanic glass-rich tuffs, and perlitic facies. The emplacement of these volcanic products was influenced by regional fault systems that provided pathways for magma ascent and may have subsequently facilitated hydrothermal fluid circulation and alteration (Hernandez 1983 ; El Bakkali 1995 ; El Bakkali et al. 1998 ; El Bakkali et al. 2001 ; Ddani et al. 2005 ; Aalaoul et al. 2015). Within this volcanic setting, bentonite formation is related to the hydrothermal and post-volcanic alteration of volcanic ash, tuff, and glass-rich volcanic materials, leading to the development of smectite-rich clay assemblages (Hernandez and Bellon 1985 ; Ddani et al. 2005 ; Aalaoul et al. 2015 ; Ait Hmeid et al. 2021a).

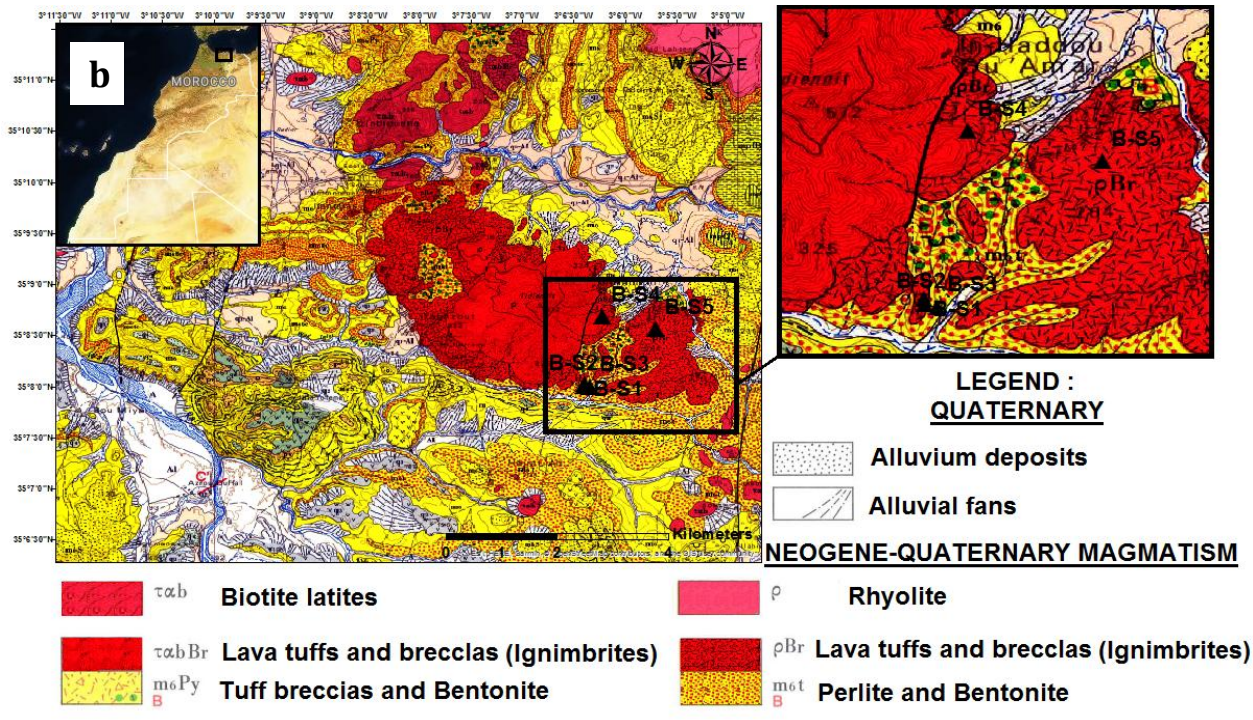
The studied bentonite samples were collected from the western flank of the Tidiennit massif, where the bentonitic outcrops are spatially associated with rhyolitic and perlitic rocks. At the outcrop scale, perlite occurs locally to the south and rhyolite to the north of the bentonitic horizons, indicating a close spatial relationship between the bentonite and its acidic volcanic host rock **(Figure 2b)**. The bentonite is interpreted to have formed through the hydrothermal and post-volcanic alteration of volcanic materials, including volcanic ash, tuffs, and glass-rich

pyroclastic products (Aalaoul et al. 2015 ; Ait Hmeid et al. 2019). Locally, the bentonite outcrops exhibit dendritic oxide precipitates on the surface and/or within the clay material, characterized by branching or tree-like morphologies **(Figure 3)**. These features are interpreted as secondary mineral precipitates rather than primary constituents of the bentonite clay assemblage and may reflect localized fluid–rock interaction and redox conditions during the alteration process.

The studied bentonite occurrence is located less than 10 km from the barite mineralization of Jbel Ouichane. Previous studies have interpreted the Jbel Ouichane barite deposits as epigenetic mineralization related to the circulation of meteoric waters mixed with ascending magmatic–hydrothermal fluids associated with Miocene intrusive activity (Dumanska-Slowik et al. 2021). This spatial proximity places the studied bentonites within a broader volcanic–hydrothermal context; however, a direct genetic relationship between the bentonite and the Jbel Ouichane barite mineralization cannot be established solely on the basis of their geographic proximity. The collected bentonite samples were therefore subjected to detailed physicochemical, mineralogical, and geochemical characterization to investigate their composition and the processes associated with their formation.



197



198

199 *Figure 2. (a) Simplified geological map of the Eastern Rif, northeastern Morocco, showing the*
200 *main geological units, massifs, tectonic structures, volcanic formations, faults, and*
201 *hydrographic network (modified from Faure-Muret 1994; Guillemin 1983). (b) Geological map*

of Jbel Tidiennt showing the sampling locations of bentonite, extracted from the geological map of the Rif region (Zeghanghane sheet; scale 1:50,000).

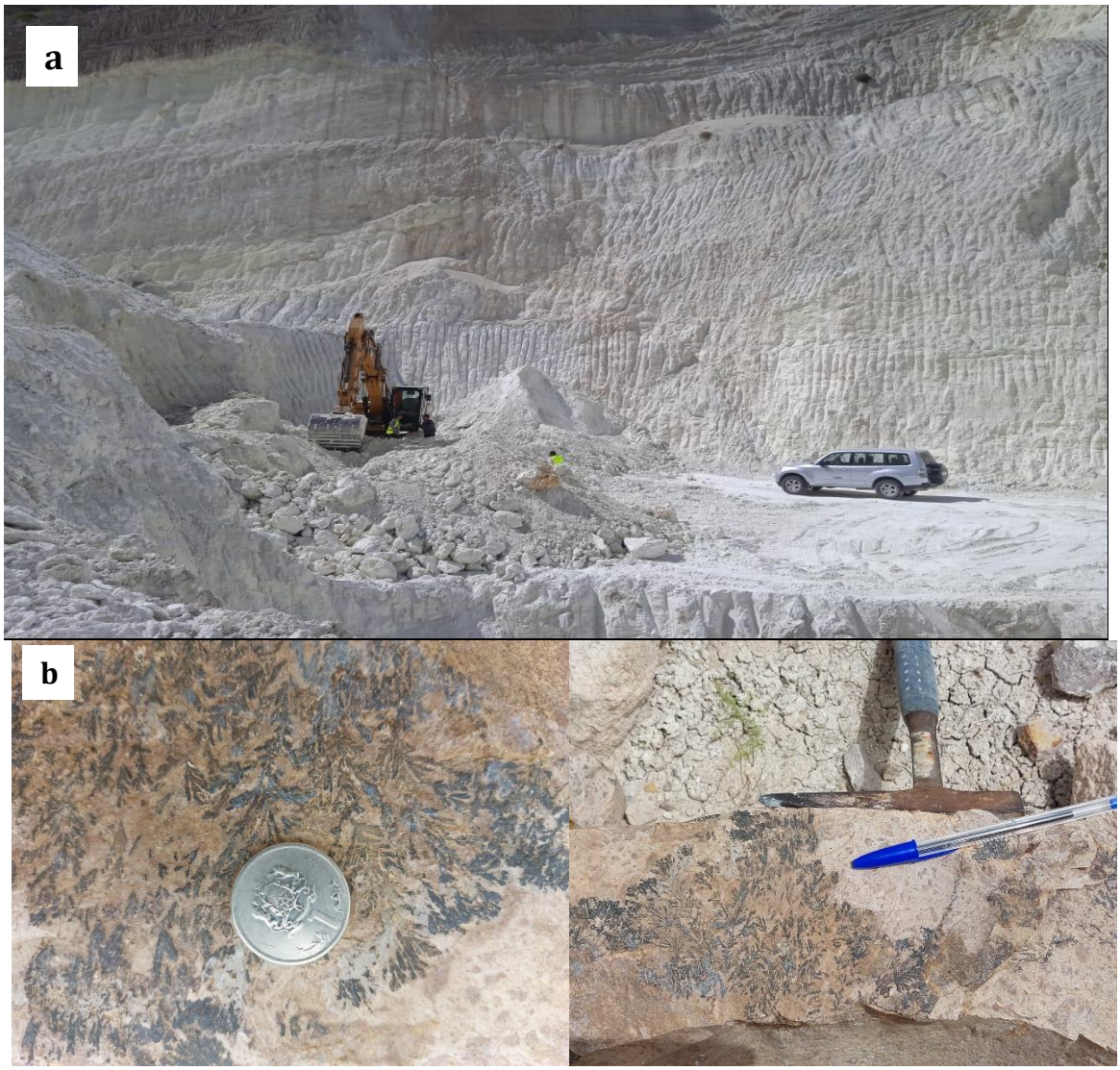


Figure 3. (a) Field photographs of bentonite deposits; (b) Plan view of bentonite showing dendritic manganese oxide patterns resembling branches or "flowers," characteristic of crystal growth processes.

III- Materials and Methods

1- Sample Collection

Five bentonite samples were collected from different locations across the Jbel Tidinnet area. Sampling was conducted along a linear transect extending between the Providencia Mine and Tribia deposits to capture the main lithological and mineralogical variations within the study

area **(Figure 4)**. The samples display a range of colors, from white to yellow, reflecting differences in alteration processes and mineralogical composition. This sampling strategy yielded a representative set of the bentonite facies occurring throughout the investigated area.

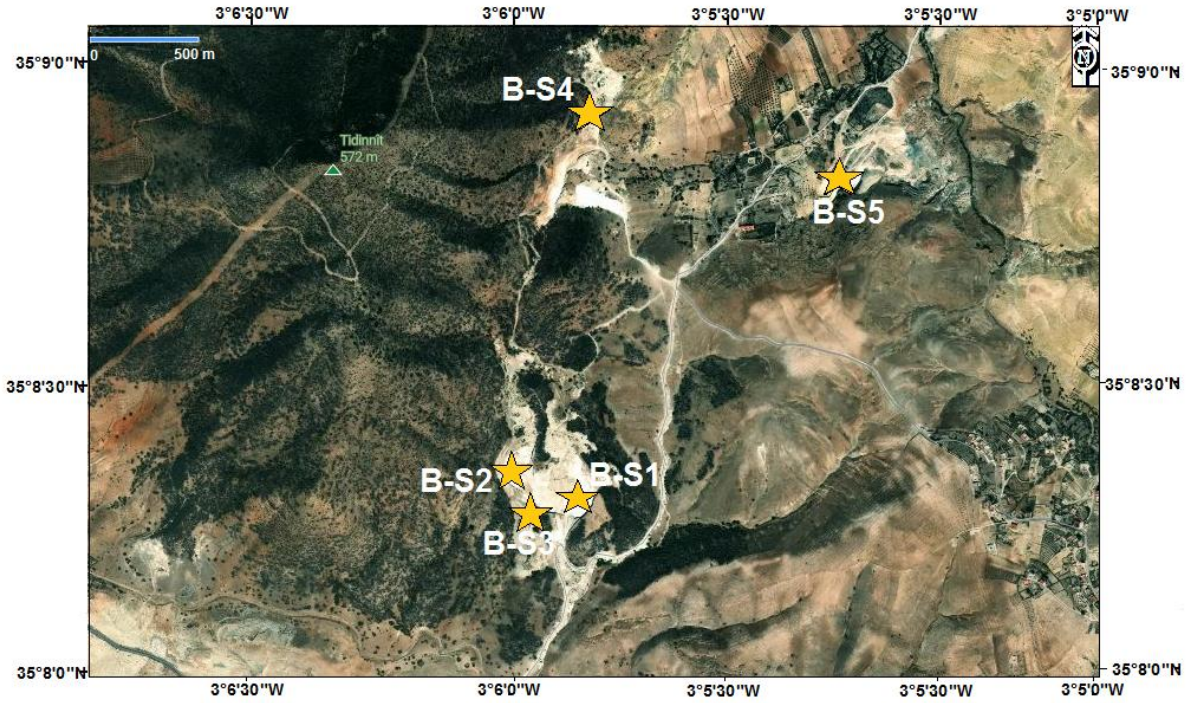


Figure 4. Locations of the sampling sites.

2- Characterization of the raw bentonite

The samples were prepared prior to their physicochemical and geochemical characterization. The samples were oven-dried at 48 °C for 24 h, then crushed using a mortar and ground in a Retsch RM200 grinder to obtain a fine and homogeneous powder.

Particle size distribution was determined by laser diffraction granulometry, in accordance with ISO 13320:2020. The granulometric parameters were calculated using the following equations: the coefficient of uniformity ($Cu=D_{60}/D_{10}$), the coefficient of curvature ($C_c=D^2_{30}/(D_{10}\times D_{60})$), and the span ($Span=(D_{90}-D_{10})/D_{50}$). The particle-size fractions were calculated from the cumulative volume-based particle size distribution obtained by laser diffraction.

The calcium carbonate ($CaCO_3$) content was determined using the calcimetric method, in accordance with the French standard NF P 94-048 (AFNOR 1996).

The pH of the samples was measured in a 10% (w/v) bentonite suspension prepared with distilled water at 25 °C. The suspension was continuously stirred using a magnetic stirrer for 4 h to ensure homogenization and promote the dissolution of ionic species. The pH was subsequently measured using a previously calibrated potentiometric electrode (Jackson 1969, Fletcher and Sposito 1989, Sposito 1989). Electrical conductivity (EC) was also determined in a 5% (w/w) aqueous bentonite suspension at a reference temperature of 25 °C (Moussout et al. 2020). Moisture content was determined gravimetrically by drying the samples at 105 °C until constant mass was reached, following ISO 11465:2025 (ISO, 2025). Loss on ignition (LOI) was determined by calcining the samples at 950 °C for 2 h, as described by Heiri et al. (2001). After cooling, the calcined samples were weighed, and the mass loss was calculated according to the following equation: LOI_{950} (%) = [(mass B − mass C) / mass B] × 100, where B represents the initial sample mass and C represents the sample mass after calcination. Total inorganic carbon (TIC) was subsequently estimated from the loss on ignition according to the following relationship: TIC (%) = LOI_{950} × 0.273.

The mineralogical composition of the sediment samples was determined by powder X-ray diffraction (XRD) with diffractometer operating at 40 kV and 30 mA with Cu radiation. The analyses were performed on powdered samples following the standard clay mineral analysis procedures described by Moore and Reynolds (1989). Mineral phases were identified using X'Pert HighScore software and the International Centre for Diffraction Data (ICDD) database.

Fourier-transform infrared (FTIR) spectroscopy over the wavenumber range of 400–4000 cm^{-1}. The bentonite samples were analyzed in the solid state using the KBr pellet technique. The pellets were prepared by mixing 5 wt.% of finely ground, dried bentonite with 95 wt.% of dried potassium bromide (KBr).

Thermal analysis was performed a thermal analyzer at a heating rate of 5 °C/min up to 1000 °C under a controlled helium atmosphere.

The cation exchange capacity (CEC) was determined using the copper–triethylenetetramine (Cu-TET) method, following established procedures for clay minerals (Ammann et al. 2005 ; Stanjek and Künkel 2016). Approximately 0.15 g of dried sample was suspended in 30 mL of a 3.33 mmol L^{-1} Cu-TET solution in the presence of $CaCO_3$ to limit carbonate dissolution. The

use of calcite-buffered copper–triethylenetetramine solutions is particularly relevant for calcareous clay samples (Ammann 2003 ; Ammann et al. 2005).

The determination of soluble and exchangeable cations, as well as soluble anions, was performed in duplicate after contacting the samples with a $CaCO_3$-buffered solution to promote the exchange of cations retained on the exchange sites of the clay phase. Following treatment, the resulting solutions were analyzed to determine the concentrations of Na^+, K^+, Ca^{2+}, Mg^{2+}, and Ba^{2+}. Sodium (Na^+) and potassium (K^+) concentrations were determined by flame atomic emission spectrometry (F-AES), whereas calcium (Ca^{2+}), magnesium (Mg^{2+}), and barium (Ba^{2+}) concentrations were measured by inductively coupled plasma optical emission spectrometry (ICP-OES), following established procedures for elemental analysis (U.S. EPA 1994). Chloride (Cl^-), considered the main soluble anion analyzed, was determined by ion chromatography (IC), following the principles described in ISO 10304-1 (ISO 2007).

Ionic concentrations were expressed in cmolcc kg^{-1} to facilitate comparison of ionic charges among the different samples. The sum of the measured cations (ΣCat.) was calculated from the concentrations of Na^+, K^+, Ca^{2+}, Mg^{2+}, and Ba^{2+} expressed as charge equivalents, while an apparent ionic balance was calculated as the difference between the measured cationic and anionic charges (ΣCat. − ΣAnion). Finally, the soluble salt content was expressed as a NaCl equivalent to facilitate comparison of salinity levels among the different bentonite samples.

The major-element chemical composition was determined by X-ray fluorescence (XRF) spectrometry after preparation of the samples as lithium tetraborate (Li-tetraborate) fused beads, in accordance with DIN EN ISO 12677 (ISO 2011). The concentrations of the major oxides, including SiO_2, Al_2O_3, Fe_2O_3, TiO_2, MgO, CaO, Na_2O, K_2O, and SO_3, were determined and expressed as weight percentages (wt.%).

For trace-element analysis, the bentonite samples were subjected to acid digestion using a mixture of hydrochloric acid (HCl), nitric acid (HNO_3), perchloric acid ($HClO_4$), and hydrofluoric acid (HF), following established procedures for the decomposition of silicate materials (USEPA 1996). The resulting digests were subsequently analyzed by inductively coupled plasma optical emission spectrometry (ICP-OES) and inductively coupled plasma mass spectrometry (ICP-MS) to determine the concentrations of the analyzed elements, using established analytical methods (USEPA 1994 ; 1996). The trace-element concentrations were expressed in mg kg^{-1}.

3- Soda Ash Activation

3.1 Calculation of Soda Ash Requirements for Sodium Activation

The sodium activation of bentonite using sodium carbonate (Na_2CO_3) is widely employed to modify its physicochemical and rheological properties (Grim 1968, Luckham and Rossi 1999, Önal 2006). In this study, the amount of Na_2CO_3 required for the sodium activation of the bentonite samples was estimated using two approaches: (**i**) the cation exchange capacity (CEC) and the exchangeable sodium content (Na^+), and (**ii**) the total content of divalent cations (Ca^{2+} and Mg^{2+}), including both exchangeable and soluble fractions.

For each sample, the soda ash dosages calculated using both approaches were compared. The higher of the two calculated dosages was selected as the final Na_2CO_3 dosage to ensure sufficient sodium activation while accounting for the potential contribution of divalent cations. The calculated dosages were expressed as mass percentages of Na_2CO_3 relative to the dry mass of bentonite.

3.1.1. Approach Based on CEC and Exchangeable Sodium

The first approach was based on the difference between the cation exchange capacity (CEC) and the initial exchangeable sodium content ($Na^+_{ex}c_h$) of the bentonite samples. This approach aims to estimate the amount of sodium carbonate required to compensate for the exchange capacity not initially balanced by exchangeable sodium, thereby increasing the proportion of sodium in the exchange complex and potentially improving the swelling and dispersion properties of the bentonite.

The amount of sodium carbonate (Na_2CO_3) required to achieve a target activation degree of 110% was estimated based on the exchange capacity not already compensated by exchangeable sodium (Na^+_{exch}), according to Equation (1) (Bahranowski et al. 2021; Macheca et al. 2022) :

$$D_{CEC} = \frac{(CEC - N^+_{exch}) \times 1.10 \times M(Na_2CO_3)}{2 \times 1000} \quad (1)$$

The equation (1) gives the Na_2CO_3 requirement in g/kg of dry bentonite, provided that the CEC and exchangeable sodium content are expressed in $cmol_c/kg$.

To express the dosage as a mass percentage:

316 $$D_{CEC}\,(\%) = \frac{D_{CEC}}{10}$$

317 **Where:**

318 $\mathbf{D_{CEC}}$: Sodium carbonate dosage calculated using the cation exchange capacity (CEC) and exchangeable
319 sodium content, expressed in g/kg of dry bentonite.

320 **CEC** : cation exchange capacity, expressed in $cmol_c/kg$;

321 $\mathbf{Na^{+}_{exch}}$: exchangeable sodium content, expressed in $cmol_c/kg$;

322 **1.10** : factor corresponding to an activation degree of 110%;

323 **$M(Na_2CO_3)$ =106 g/mol**: molar mass of sodium carbonate;

324 **1000**: unit conversion factor.

325

326 This approach is based on the principle of modifying the exchangeable cation composition of
327 bentonite to increase sodium saturation and influence its swelling and dispersion behavior
328 (Grim 1968, Luckham and Rossi 1999).

329

330 **2. Approach Based on Divalent Cations (Ca^{2+} and Mg^{2+})**

331 The second approach was based on the stoichiometric requirement of sodium carbonate for the
332 precipitation of divalent cations, particularly Ca^{2+} and Mg^{2+}, as carbonates. The calculation
333 considered the total content of these cations, including both exchangeable and soluble fractions.
334 This approach was used to estimate the additional soda ash requirement associated with divalent
335 cations that may influence the physicochemical properties of bentonite during sodium
336 activation.

337 The total divalent cation content was determined by combining the exchangeable and soluble
338 fractions of Ca^{2+} and Mg^{2+}. The theoretical Na_2CO_3 requirement associated with these divalent
339 cations was then calculated using Equation (2), based on the stoichiometric relationship
340 between divalent cations and sodium carbonate during bentonite activation. This calculation
341 accounts for the potential contribution of calcium and magnesium to soda ash consumption
342 during the conversion of calcium-rich bentonite into its sodium-activated form (Karagüzel et
343 al. 2010 ; Mahmoud et al. 2019).

344 $$\mathbf{D_{Ca+Mg}\,(\%)} = \frac{\sum \boldsymbol{Ca^{2+}, Mg^{2+}}\ \boldsymbol{(Cmol_c/Kg)} \times \boldsymbol{MNa_2CO_3}}{\mathbf{2 \times 1000 \times 10}} \qquad (2)$$

The consideration of calcium and magnesium is relevant because divalent cations influence the physicochemical behavior of bentonite suspensions, while carbonate addition may contribute to calcium removal through precipitation under suitable chemical conditions (Luckham and Rossi 1999).

IV- RESULTS

1- Particle-Size Distribution

Table 1 presents the percentages of the different grain-size fractions and the main grain-size parameters of the studied samples. According to the commonly used granulometric classification (Wentworth 1922), the studied materials contain three grain-size fractions in different proportions: clay, silt, and sand.

The granulometric results show a clear dominance of the silt fraction, which ranges from 54.21 to 73.98%, followed by the sand fraction (21.14–43.79%). The clay fraction remains low, ranging from 1.99 to 5.04%.

The grain-size parameters show differences in particle-size distribution between the samples. The median grain diameter (D50) ranges from 28.48 to 51.63 µm. The highest D50 values are observed in B-S1 to B-S3, indicating relatively coarser materials. In contrast, B-S4 and B-S5 have lower D50 values, indicating relatively finer materials. The D90 values range from 89.76 to 263.71 µm and also show a wide variation in particle sizes, especially for B-S1, which has the highest D90 value (263.71 µm).

The uniformity coefficient (Cu) ranges from 11.15 to 13.71, indicating a relatively wide grain-size distribution **(Figure 5a)**. The Cc values, ranging from 1.10 to 1.23, suggest a relatively well-graded distribution of intermediate particle sizes. Finally, the Span values range from 2.47 to 5.41, confirming a greater dispersion of particle sizes in some samples, particularly B-S1, which shows the highest value, while B-S3 exhibits the lowest dispersion (ASTM Committee D-18 on Soil and Rock 2017 ; Davarpanah 2025). It can be observed that all the materials studied exhibit a loam texture for samples B-S1, B-S2, and B-S3, and a sandy loam texture for samples B-S4 and B-S5 **(Figure 5b)**.

Table 1. Particle-size distribution and granulometric parameters of the bentonite samples.

Sample	Clay (%)	Silt (%)	Sand (%)	D10 (µm)	D30 (µm)	D50 (µm)	D60 (µm)	D90 (µm)	C_u	C_c	Span
B-S1	3.03	54.58	42.39	6.17	21.64	47.58	68.73	263.71	11.15	1.11	5.41
B-S2	2.00	54.21	43.79	6.18	23.04	51.63	70.01	136.34	11.33	1.23	2.52
B-S3	1.99	54.30	43.71	6.09	22.65	50.58	68.34	131.23	11.22	1.10	2.47
B-S4	4.88	73.98	21.14	3.22	11.97	28.48	38.37	89.76	11.92	1.16	3.04
B-S5	5.04	67.70	27.29	3.11	12.33	30.57	42.66	129.52	13.71	1.15	4.14

Legend: Clay **<2 µm (%)**; Silt **2–63 µm (%)**; Sand **>63 µm (%)**; **Dx** = diameter corresponding to x% of the cumulative volume distribution; **Cu** = uniformity coefficient; **Cc** = coefficient of curvature; **Span** = grain-size distribution span index.

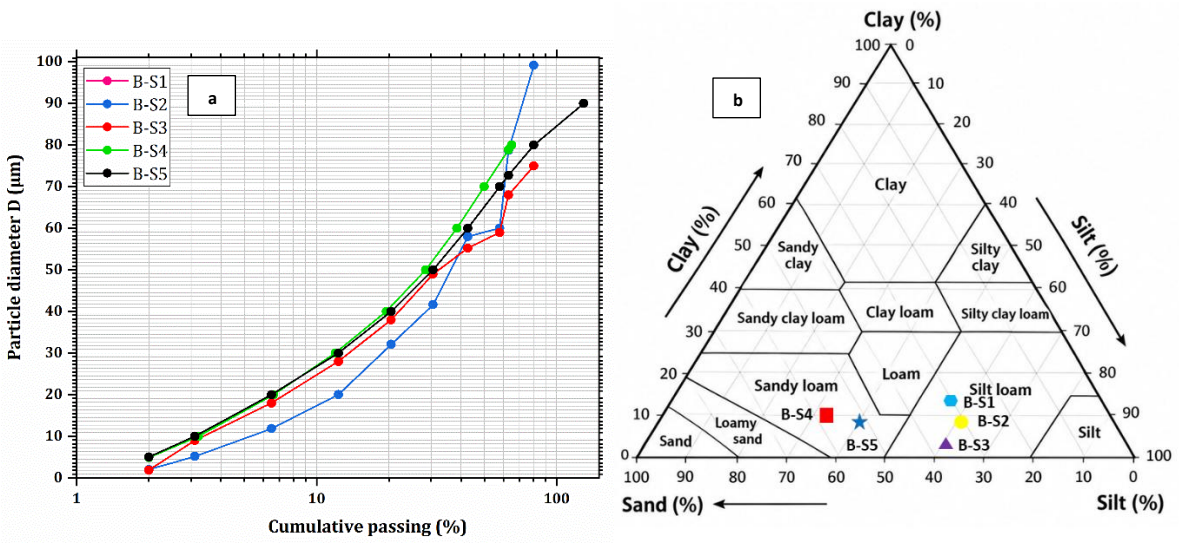


Figure 5. (a) Grain-size distribution curves of the studied bentonites; (b) textural classification of the bentonites according to the sand–silt–clay ternary diagram of Shepard (1954).

2- Physicochemical Properties

The physicochemical characterization of the five samples collected from the Jbel Tidienit deposit revealed that the studied materials are predominantly alkaline **(Table 2)**, with pH values ranging from 8.2 to 9.0 and an average value of 8.64. The $CaCO_3$ content varies between 7 and 11%, with an average of 8.33%, indicating a moderate and relatively homogeneous distribution of carbonate minerals throughout the deposit.

The cation exchange capacity (CEC) ranges from 67 to 103 cmolc kg^{-1}, with an average of 89.60 cmolc kg^{-1}, reflecting a relatively high cation exchange capacity among the analyzed

samples. CEC is primarily influenced by the mineralogical composition of the material, particularly the type and abundance of clay minerals, as well as organic matter content and pH (Ross and Ketterings 2011).

The water content varies from 7.0 to 12.5%, with a mean value of 9.86%, suggesting relatively limited variability in moisture content among the analyzed samples. Water retention is influenced by several factors, particularly the material's texture, porosity, mineralogical composition, and organic matter content (Saxton and Rawls 2006).

The loss on ignition (LOI) at 950 °C ranges from 6.0 to 8.9%, with an average of 7.60%, indicating the presence of volatile constituents, carbonate phases, and/or structurally bound water. Electrical conductivity shows significant variability, ranging from 176 to 1229 µS cm^{-1}, with an average value of 640 µS cm^{-1}, reflecting variability in the concentration of soluble salts among the analyzed bentonites.

The calculated Total Inorganic Carbon (TIC), derived from LOI at 950 °C, ranges from 1.64 to 2.43%, with an average value of 2.08%. These relatively low to moderate values indicate a limited but consistent presence of inorganic carbon, mainly associated with carbonate minerals.

Variations in TIC broadly follow those observed in LOI, suggesting a relationship between carbonate decomposition and inorganic carbon content. In addition, the consistency between TIC and $CaCO_3$ results supports the interpretation that carbonate minerals occur in a dispersed form rather than as dominant phases. This distribution may influence the reactivity, buffering capacity, and overall geochemical behavior of the materials (Loeppert and Suarez 1996).

Overall, the materials from the Jbel Tidienit deposit are characterized by alkaline pH, moderate carbonate content, relatively high CEC, and variable salinity. These physicochemical characteristics indicate potential relevance for industrial and environmental applications, although their specific suitability would require further application-oriented evaluation.

Table 2: Major physicochemical properties of bentonites.

Sample	$CaCO_3$ (%)	pH	CEC (cmolc kg^{-1})	W (%)	LOI at 950 °C (%)	EC (µS cm^{-1})	TIC (%)
B-S1	8.00	8.30	103.00	10.8	8.5	1229	2.32
B-S2	7.00	8.70	94.00	10.0	7.9	176	2.16
B-S3	8.00	8.20	92.00	12.5	8.9	780	2.43

B-S4	8.00	9.00	83.00	9.0	6.7	399	1.83
B-S5	8.00	9.00	67.00	7.0	6.0	616	1.64
Average	**7.80**	**8.64**	**87.80**	**9.86**	**7.60**	**640**	**2.08**

Note: CEC = cation exchange capacity; LOI = loss on ignition; W = water content; EC = electrical conductivity; TIC = total inorganic carbon.

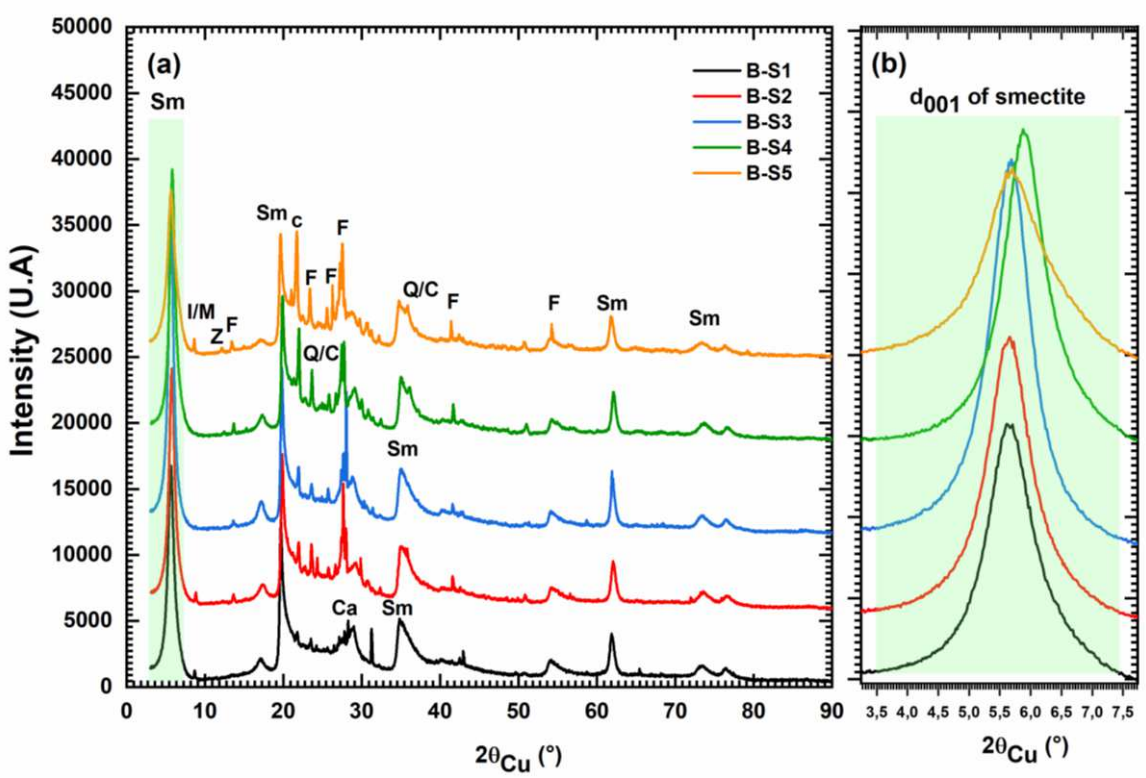
3- Mineralogical Composition by XRD

Figure 6 presents the X-ray diffraction (XRD) patterns of the studied materials. The XRD results indicate that the samples are predominantly composed of smectite, with contents ranging from 58 to nearly 89 wt.% (**Figure 7**). The smectite phase is associated with minor amounts of other mineral phases, including illite/mica (0.5–1.5 wt.%), zeolite (0.5–3.5 wt.%), quartz/cristobalite (1.1–14.2 wt.%), feldspars (8.5–22.1 wt.%), and calcite (0.3–6 wt.%). These minerals occur as accessory phases within the predominantly smectitic assemblage.

The basal (001) reflection of smectite occurs at approximately 15.5 Å. This basal spacing is probably consistent with a hydrated smectite containing divalent exchangeable cations, mainly Ca^{2+} and Mg^{2+}, in the interlayer space (Ferrage et al. 2007 ; García-Romero et al. 2021).

The d(060) reflection, located at approximately 1.465 Å, provides additional information on the octahedral character of the smectite and is consistent with a dioctahedral smectite (U.S. Geological Survey 2001 ; Delavernhe et al. 2015).

Overall, the XRD results show that smectite is the dominant mineral phase, while quartz/cristobalite, feldspars, illite/mica, zeolite, and calcite occur as accessory phases. The high smectite content is also consistent with the relatively high CEC values measured in the studied materials.



433

434 *Figure 6. (a) X-ray diffraction (XRD) patterns of the bentonite samples investigated; (b)*

435 *intensity and position of the (001) basal reflections of smectite.*

436 **Note: Sm** = smectite; **I/M** = illite/mica; **Z** = zeolite; **Q/C** = quartz/cristobalite; **F** = feldspar; **C** = calcite.

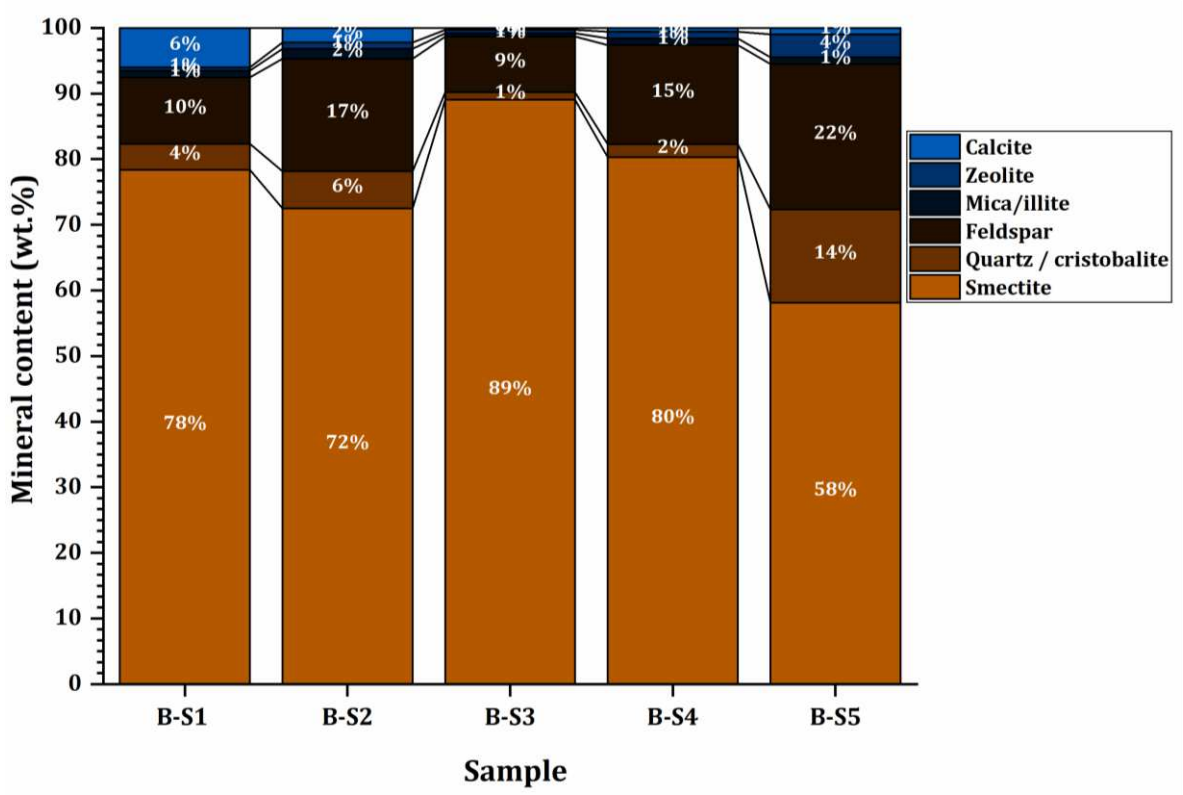


Figure 7. Main Mineralogical Composition of the Studied Samples (wt.%).

4- FTIR Spectroscopy

The FTIR spectroscopic analysis of the samples highlights several absorption bands characteristic of the structure of smectites, particularly montmorillonite (**Figure 8**). The band located around 3620 cm^{-1} is assigned to the stretching vibration ν(Al_2–OH) of structural hydroxyl groups associated with the octahedral sites of montmorillonite. An intense band observed at 3414 cm^{-1} is attributed to the stretching vibrations ν(O–H) of adsorbed and/or interlayer water molecules, indicating the presence of water within the structure. When observed, the band located around 1630–1640 cm^{-1} can be associated with the bending vibration (δH_2O) of molecular water associated with the clay surfaces and interlayer spaces (Madejová and Komadel 2001 ; Madejová 2003 ; Frinak et al. 2005).

In the low-frequency region, an intense absorption band centered at 1035.70 cm^{-1} is assigned to the stretching vibration ν(Si–O), characteristic of the silicate framework of phyllosilicates (Madejová et al. 2010). This band may also be influenced by the presence of silica phases and feldspars. The band observed at 916 cm^{-1} is attributed to the bending vibration δ(Al_2–OH). Its development constitutes a characteristic indication of the presence of montmorillonite and reflects the contribution of Al cations in the octahedral sites of smectites. A shoulder observed around 886 cm^{-1} may be associated with δ(Al–Fe–OH) bending vibrations, indicating the presence of Fe in the octahedral environment of the smectitic structure. In addition, δ(Al–Mg–OH) vibrations are weakly expressed in the studied samples; a weak shoulder around 845 cm^{-1}, better resolved after spectral deconvolution, may be attributed to the presence of Mg in the octahedral sites (Vantelon et al. 2001).

The region between 780 and 800 cm^{-1} is associated with silica phases. In particular, a doublet located around 799 and 780 cm^{-1} is generally characteristic of quartz, whereas a single band around 798–800 cm^{-1} may be associated with cristobalite or amorphous silica. This contribution may also be related to the presence of opal-CT, whose structure contains domains related to cristobalite and tridymite. However, precise identification of the silica phase requires consideration of all the characteristic bands in the spectrum, together with the results obtained from other characterization techniques. The band observed around 700.16 cm^{-1} may be attributed to vibrations of M^{IV}–OH bonds, where M represents the Al, Mg, and Fe cations occupying the octahedral sites (Plevova et al. 2020 ; Michalski et al. 2003).

A band located around 616 cm^{-1} may be associated with a bending vibration δ related to the structure of the silicate layers of smectites and may provide information on the structural environment and the contribution of the tetrahedral layer. The band located at 518 cm^{-1} is assigned to a bending vibration of Si–O bonds, particularly vibrations involving Si–O–Al bonds. Finally, the band observed around 458 cm^{-1} may be attributed to bending vibrations of the silicate framework, particularly vibrations of Si–O–Al bonds, which are characteristic of the structure of phyllosilicates (Madejová and Komadel 2001 ; Bishop et al. 2002).

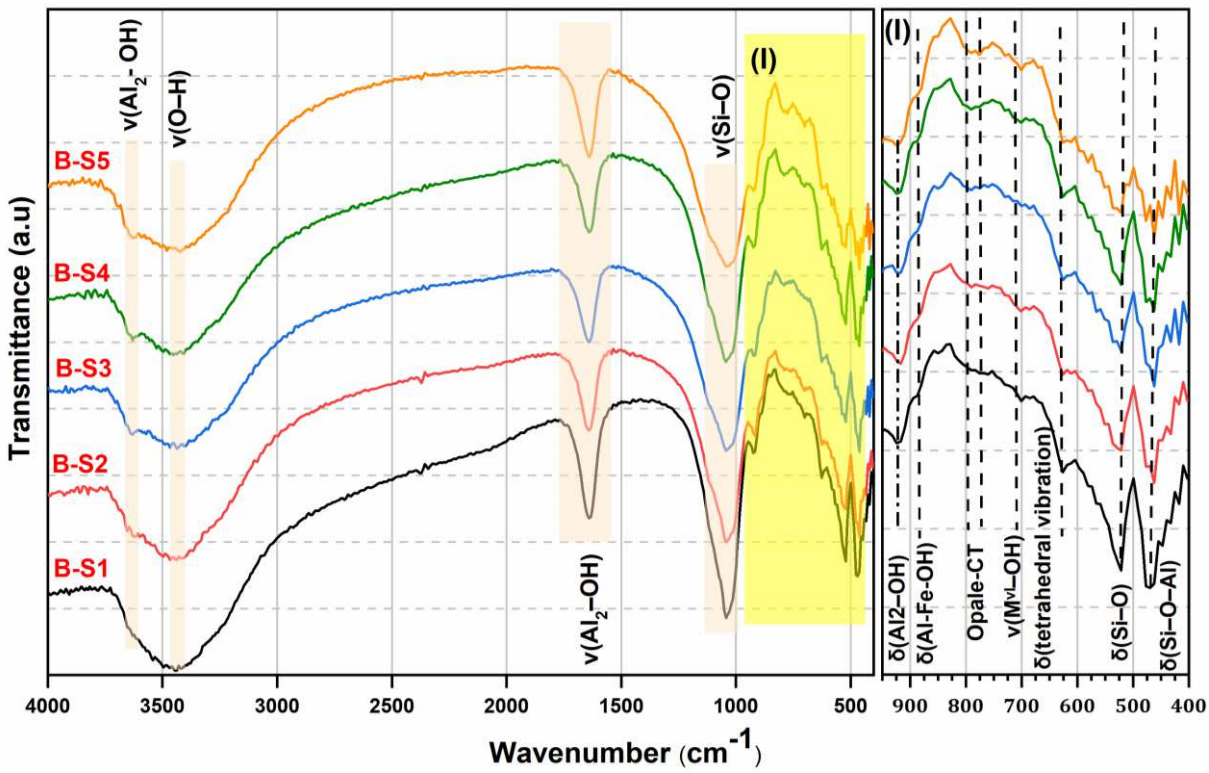


Figure 8. FTIR spectra of the studied samples recorded in the wavenumber range of 400–4000 cm^{-1}.

5- Soluble and Exchangeable Cations

The concentrations of soluble and exchangeable cations show notable variability among the analyzed samples (**Table 3**). Na^+ concentrations range from 24.0 to 46.0 cmolc kg^{-1}, with the maximum value recorded in B-S1 and the minimum in B-S2. K^+ occurs at relatively low and slightly variable concentrations, ranging from 1.4 to 3.3 cmolc kg^{-1}. Ca^{2+} concentrations range from 20.0 to 35.0 cmolc kg^{-1}, whereas Mg^{2+} represents one of the major cations measured, with concentrations ranging from 28.0 to 46.0 cmolc kg^{-1}. Ba^{2+} occurs at very low concentrations, ranging from <0.01 to 0.09 cmolc kg^{-1}, with the maximum value observed in B-S4 (**Figure 9 a**).

The contribution of Na^+ to the sum of the measured cations (ΣCat.) ranges from 24.0 to 42.2% among the samples, corresponding to 35.1% for B-S1, 24.0% for B-S2, 35.8% for B-S3, 30.8% for B-S4, and 42.2% for B-S5. The divalent cations Mg^{2+} and Ca^{2+} also account for a substantial fraction of the total cationic composition. Mg^{2+} consistently exhibits higher concentrations than Ca^{2+} in all samples, with particularly pronounced differences in B-S3 and B-S5. In contrast, K^+ and Ba^{2+} represent minor fractions of the total measured cations. The occurrence and relative proportions of these cations are consistent with the variable exchangeable-cation composition commonly reported for bentonites and smectite-rich materials (Carroll 1959).

The concentration of soluble Cl^- ranges from 0.6 to 6.5 cmolc kg^{-1}, with the maximum value observed in B-S1 and the minimum in B-S2. The corresponding NaCl equivalent contents range from 0.03 to 0.38 wt.%, with the highest value recorded for B-S1 and the lowest for B-S2. This variation highlights significant differences in the amount of soluble salts among the studied bentonites.

The sum of the measured cations (ΣCat.) ranges from 90.0 to 131.0 cmolc kg^{-1}, with the maximum value recorded for B-S1 and the minimum for B-S5. These values are higher than the CEC values measured for the corresponding samples (**Figure 9 b**).

The measured concentrations correspond to soluble and exchangeable cations released during the treatment and therefore do not exclusively represent cations associated with the exchange complex. The difference observed between ΣCat. and CEC may thus be explained, at least in part, by the presence of cations in the soluble fraction of the bentonites, particularly in the form of soluble salts.

The difference between ΣCat. and ΣAnion ranges from 88.3 to 124.5 cmolc kg^{-1} among the samples. This difference indicates an apparent excess of measured cationic charge relative to the anionic charge represented by the quantified Cl^-. However, this parameter does not represent a complete ionic charge balance, since other potentially present anions, such as SO_4^{2-} and HCO_3^-, were not quantified. Previous studies on bentonite characterization have shown that incomplete anion analyses can lead to discrepancies in charge balance and complicate the distinction between soluble and exchangeable cations (Bradbury and Baeyens 2003 ; Dohrmann et al. 2012). Therefore, the calculated difference should be interpreted as an apparent charge imbalance based on the measured ionic species, rather than as a direct estimate of the exchangeable cation fraction.

The NaCl equivalent concentrations range from 0.51 to 6.50 cmolc kg^{-1}, with the highest value recorded for B-S1 (6.50 cmolc kg^{-1}) and the lowest for B-S2 (0.51 cmolc kg^{-1}).

Overall, the cationic composition is mainly characterized by Na^{+}, Mg^{2+}, and Ca^{2+}, which represent the principal species measured in the five bentonites. The soluble salt fraction also shows marked variability among the samples. B-S1 is characterized by the highest concentrations of Na^{+} (46.0 cmolc kg^{-1}), Mg^{2+} (46.0 cmolc kg^{-1}), ΣCat. (131.0 cmolc kg^{-1}), and Cl^{-} (6.5 cmolc kg^{-1}), as well as the highest NaCl equivalent concentration (6.50 cmolc kg^{-1}). In contrast, B-S2 exhibits the lowest concentrations of Na^{+} (24.0 cmolc kg^{-1}), Cl^{-} (0.6 cmolc kg^{-1}), and NaCl equivalent (0.51 cmolc kg^{-1}).

Figure 10 shows a strong positive relationship between NaCl equivalent concentration and electrical conductivity (EC) in the analyzed bentonites. A linear regression yielded an R^2 value of 0.921, indicating a strong association between soluble salt content and electrical conductivity.

Table 3. Concentrations of soluble and exchangeable cations, soluble chloride, and NaCl equivalent in the analyzed bentonites.

Sample	Na^{+}	K^{+}	Ca^{2+}	Mg^{2+}	Ba^{2+}	ΣCat.	Cl^{-}	ΣCat. − ΣAnion	NaCl equivalent
B-S1	46.0	2.9	35.0	46.0	<0.01	131.0	6.5	124.5	6.50
B-S2	24.0	3.1	28.0	45.0	0.06	100.0	0.6	99.4	0.51
B-S3	39.0	3.3	24.0	43.0	<0.01	109.0	2.6	106.4	2.57
B-S4	28.0	1.4	28.0	33.0	0.09	91.0	1.1	89.9	1.03
B-S5	38.0	2.9	20.0	28.0	0.07	90.0	1.7	88.3	1.71

Note: All concentrations are expressed in cmolc kg^{-1}. ΣCat. = sum of measured cationic charges; ΣCat. − ΣAnion = apparent ionic balance based on the difference between measured cationic and Cl^{-} anionic charges; NaCl equivalent = soluble salt content expressed as NaCl equivalent. <0.01 = below the reported detection/quantification limit.

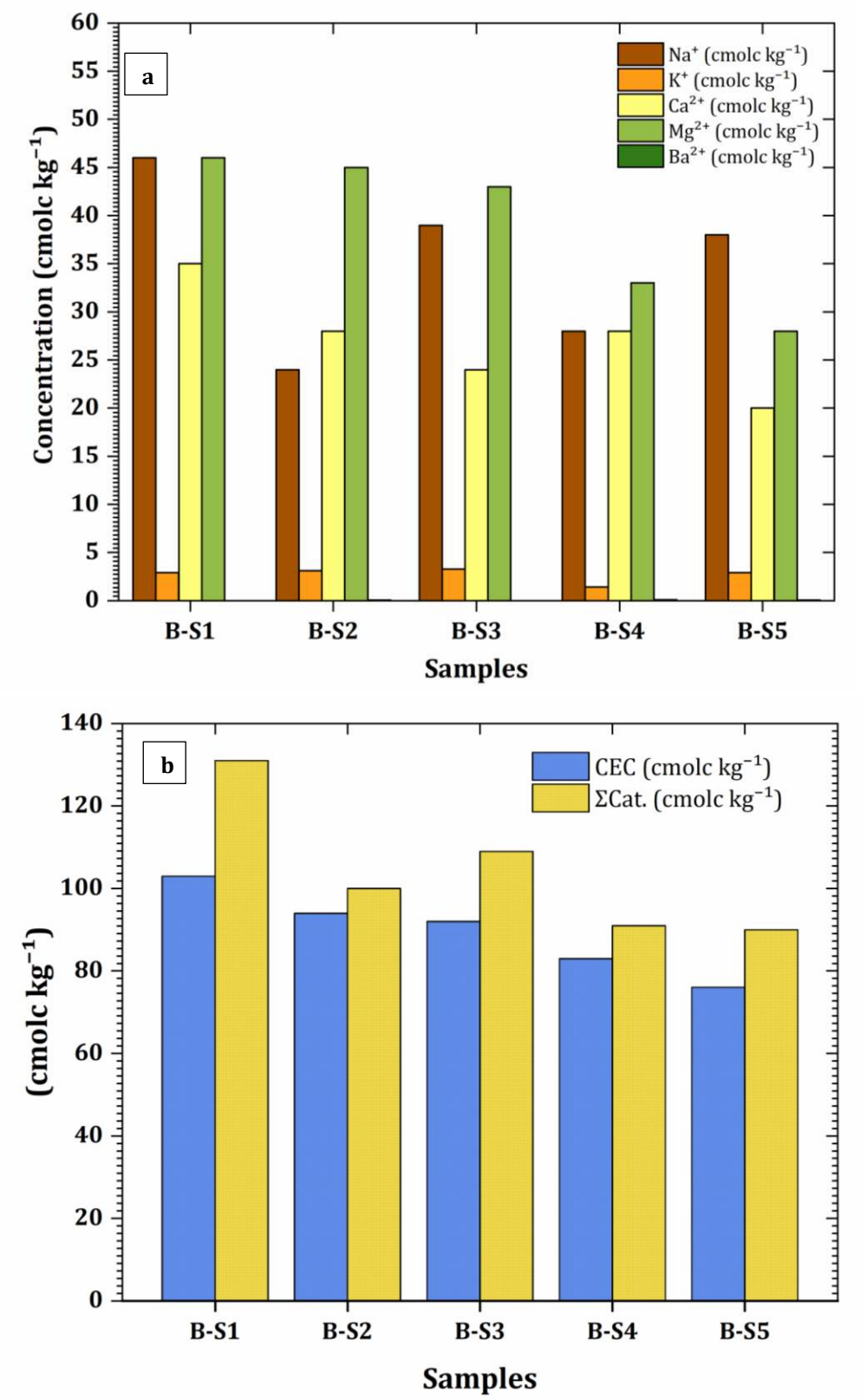


Figure 9. (a) Distribution of the main exchangeable cations (Na^+, K^+, Ca^{2+}, Mg^{2+}, and Ba^{2+}) in the analyzed bentonites; (b) Comparison between cation exchange capacity (CEC) and total exchangeable cations (ΣCat.).

The PCA biplot further highlights the relationships between the bentonite samples and their physicochemical properties (**Figure 11**). The first two principal components account for 82.2% of the total variance (Dim1: 63.7%; Dim2: 18.5%). B-S1 is associated with the direction of Na^+, Cl^-, and electrical conductivity (EC), whereas B-S4 is located on the opposite side of Dim1, closer to the Ba^{2+} and pH vectors. Samples B-S2 and B-S5 occupy distinct positions on the biplot, indicating differences in their physicochemical characteristics.

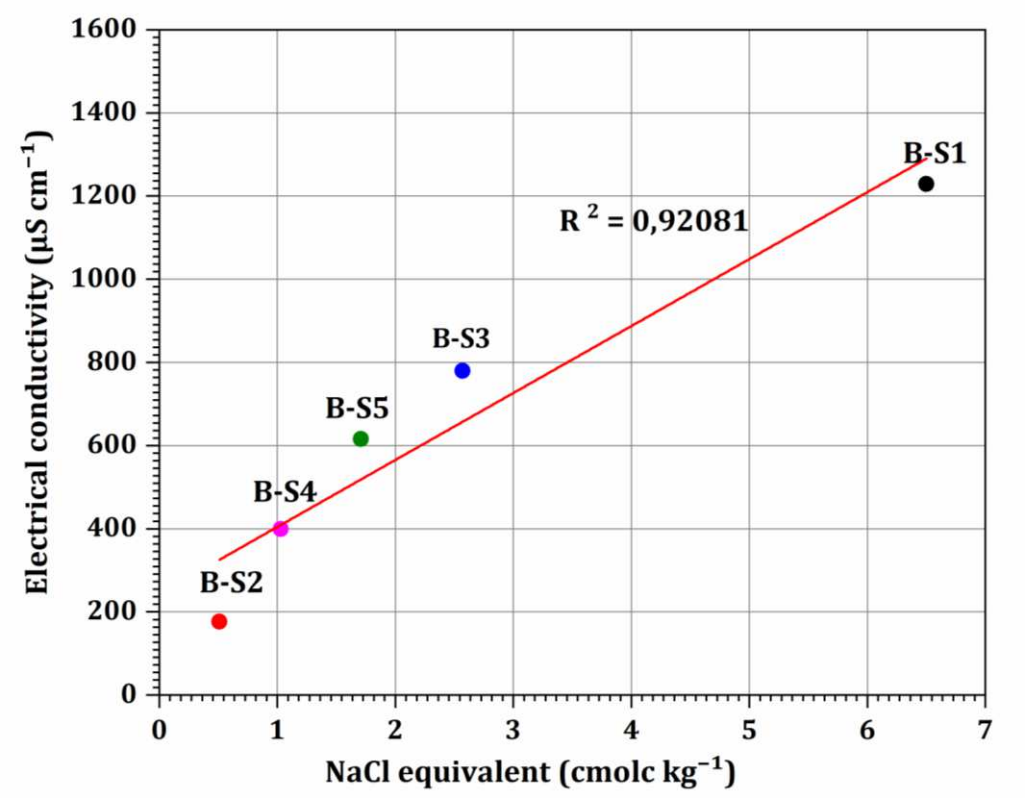


Figure 10. Linear relationship between NaCl equivalent concentration and electrical conductivity (EC) in the analyzed bentonites.

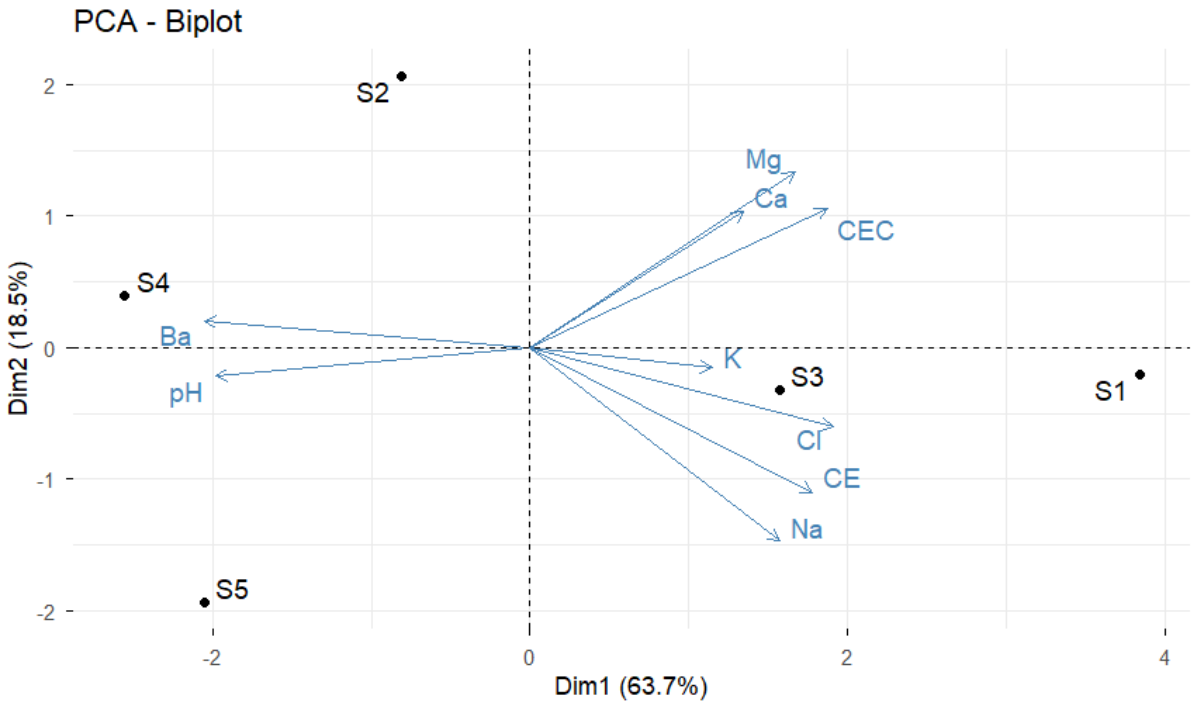


Figure 11. PCA biplot illustrating the relationships between the analyzed bentonite samples and their physicochemical properties.

6- Thermal Analysis

The thermogravimetric (TG) and derivative thermogravimetric (DTG) curves of bentonite samples B-S1 and B-S5 reveal five thermal stages (**Figure 12**):

Phase I (25–200 °C): This phase is characterized by mass loss, with a pronounced DTG peak at approximately 100–120 °C. It is mainly attributed to the removal of free and surface-adsorbed water, as well as part of the interlayer water associated with smectite minerals, particularly montmorillonite (Babiy et al. 2025). Differences in peak position and mass loss between B-S1 and B-S5 may reflect variations in water content and hydration behavior (Pret 2003 ; Derkowski and Kuligiewicz 2022 ; Babiy et al. 2025).

Phase II (200–600 °C): The gradual mass loss observed in this temperature range may be associated with the removal of residual, strongly retained water, particularly at the lower end of this interval. At higher temperatures, structural dehydroxylation of smectite minerals may begin and contribute to the mass loss, depending on their mineralogical composition and crystal structure. Minor contributions from other thermally induced mineral transformations may also occur; however, their identification requires complementary analytical data. Differences

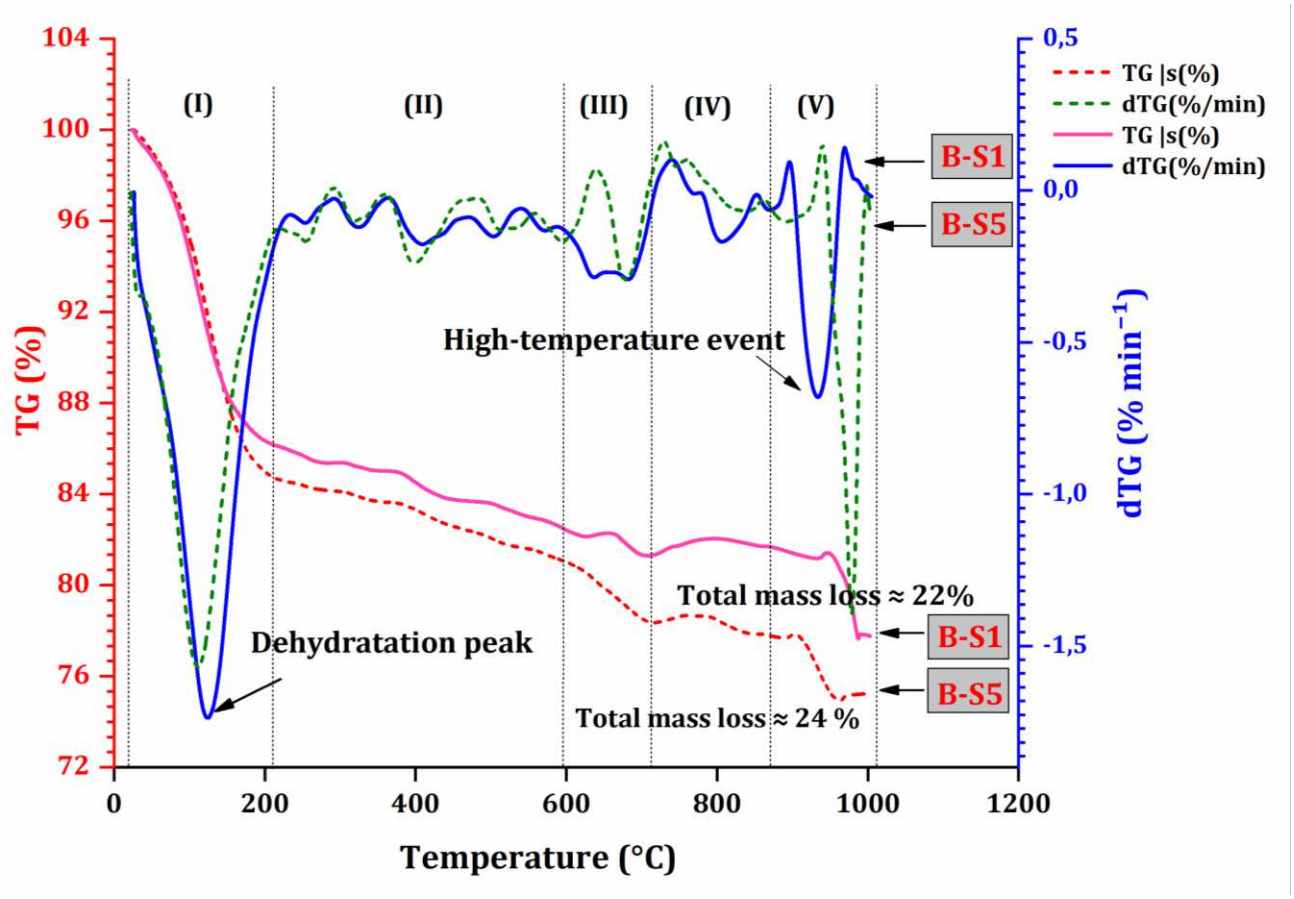
between samples B-S1 and B-S5 may reflect variations in their mineralogical composition and thermal behavior (Bish and Duffy 1990).

Phase III (600–700 °C): This stage may be associated with the continued dehydroxylation of smectite minerals, particularly montmorillonite, involving the release of structural hydroxyl groups from the octahedral sheet as water vapor. This process can progressively modify the crystal structure of the clay minerals. Differences in the DTG response between samples B-S1 and B-S5 may reflect variations in smectite composition, structural characteristics, or the extent of dehydroxylation (Lo Dico et al. 2024 ; Derkowski and Kuligiewicz 2022).

Phase IV (700–850 °C): The relatively limited mass loss observed in this temperature range, accompanied by variations in the DTG curves, may be associated with continued structural transformations following the dehydroxylation of smectite minerals (Derkowski et al. 2012). These transformations may involve structural reorganization and changes in the aluminosilicate framework, depending on the mineralogical composition of the bentonite. Differences between samples B-S1 and B-S5 may reflect variations in their thermal evolution. However, further mineralogical characterization is required to confirm the nature of these transformations (Xi et al. 2004 ; Earnest 2005).

Phase V (850–1000 °C): A marked thermal event is observed between approximately 900 and 970 °C. This event may be associated with high-temperature structural reorganization and the possible formation of new mineral phases. The contribution of carbonate decomposition, particularly calcite decomposition, should be considered only if carbonate minerals are present in the samples. These interpretations require confirmation through complementary mineralogical and chemical analyses, particularly X-ray diffraction (XRD) and chemical composition analysis (Bish and Duffy 1990 ; Benhammou et al. 2009). The broader and shifted DTG peak observed for B-S5 may reflect differences in its high-temperature thermal behavior and mineralogical composition compared with B-S1.

The total mass loss is approximately 22% for B-S1 and 24% for B-S5, indicating a slightly higher overall mass loss for B-S5.



598 *Figure 12. Thermogravimetric (TG) and derivative thermogravimetric (DTG) curves of*
599 *samples B-S1 and B-S5.*

600 **Note** : **Phase I** (25–200 °C): Dehydration; **Phase II** (200–600 °C): Residual dehydration and thermal
601 transformations; **Phase III** (600–700 °C): Dehydroxylation; **Phase IV** (700–850 °C): Structural
602 reorganization; **Phase V** (850–1000 °C): High-temperature transformations.

603 # 7- Major- and Trace-Element Geochemistry

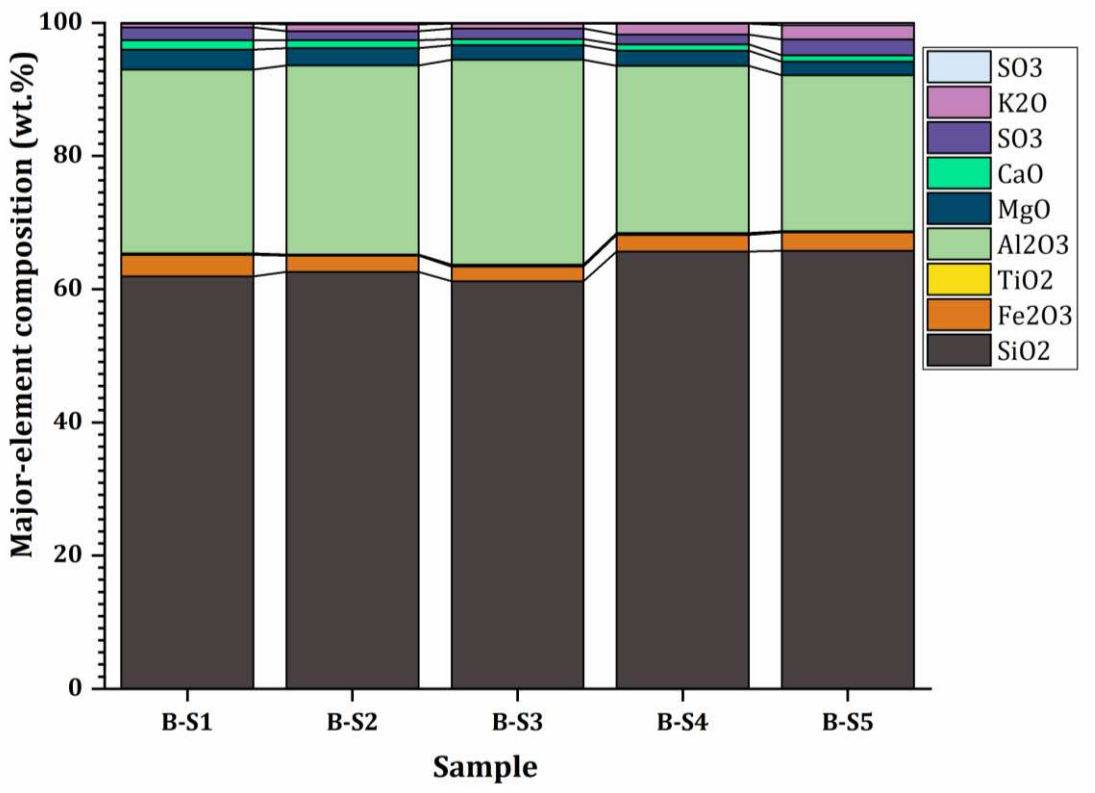
604 ## 7.1 Major Elements

605 The major-element composition of the analyzed bentonites is characterized by moderate SiO_2
606 and relatively high Al_2O_3 contents (**Table 4**). SiO_2 contents range from 55.5 to 61.2 wt.%,
607 whereas Al_2O_3 varies from 21.8 to 27.9 wt.%**.** The highest Al_2O_3 content is recorded in B-S3
608 (27.9 wt.%), while the highest SiO_2 content occurs in B-S5 (61.2 wt.%). The relatively high
609 Al_2O_3 contents are consistent with the aluminosilicate-rich composition of the studied
610 bentonites and are compatible with the presence of Al-rich clay minerals (Kogel and Lewis
611 2001) **(Figure 13)**.

612 Fe_2O_3 contents range from 2.0 to 2.9 wt.%, while TiO_2 occurs at low concentrations, ranging
613 from 0.15 to 0.25 wt.%. MgO contents vary between 1.9 and 2.7 wt.%, whereas CaO ranges
614 from 0.8 to 1.3 wt.%. Among the alkali oxides, Na_2O concentrations range from 1.24 to 2.18
615 wt.%, while K_2O varies between 0.49 and 2.02 wt.%. The highest Na_2O and K_2O contents are
616 recorded in B-S5, with values of 2.18 and 2.02 wt.%, respectively. SO_3 occurs at very low
617 concentrations, ranging from 0.11 to 0.32 wt.%.

618 *Table 4. Major-element composition of the analyzed bentonites (XRF, wt.%).*

Sample	SiO_2	Fe_2O_3	TiO_2	Al_2O_3	MgO	CaO	Na_2O	K_2O	SO_3
B-S1	56.5	2.9	0.22	25.2	2.7	1.3	1.77	0.49	0.13
B-S2	57.2	2.2	0.19	25.9	2.4	1.1	1.24	0.89	0.24
B-S3	55.5	2.0	0.25	27.9	2.0	0.8	1.47	0.66	0.11
B-S4	60.9	2.3	0.25	23.3	2.1	0.9	1.37	1.51	0.11
B-S5	61.2	2.6	0.15	21.8	1.9	0.9	2.18	2.02	0.32



619 *Figure 13. Major-element composition of the Studied Samples (wt.%).*

7.2 Trace Elements

The concentrations of trace elements measured in the studied bentonites are presented in **Table 5**. Overall, their composition is characterized by the predominance of Ba (1,140–5,360 ppm), followed by relatively elevated concentrations of Sr (124–163 ppm), Zr (139–170 ppm), and Mn (11–119 ppm). Among the other analyzed elements, Cr (7–35 ppm), Th (41–49 ppm), and Nb (19.0–22.3 ppm) exhibit relatively consistent concentrations, whereas several elements show pronounced variability among the samples. In particular, Ga concentrations range from <0.1 to 73.9 ppm, Zn from <0.5 to 182 ppm, and As from <0.5 to 13.7 ppm, indicating a heterogeneous distribution of these elements among the studied samples. The siderophile elements Co (0.6–2.5 ppm) and Ni (3.4–13.6 ppm) occur at relatively low concentrations, while most of the remaining trace elements are present at low concentrations or below their respective detection limits. Sulfur concentrations range from 0.02 to 0.11 wt.%, with the highest value recorded in sample B-S5. The observed variability, particularly in Ba, Mn, Ga, Zn, and S, may reflect differences in mineralogical composition and/or variations in the abundance and distribution of accessory mineral phases among the samples.

The marked enrichment in Ba, particularly in samples B-S2 and B-S5, deserves particular attention. Although Ba may partly reflect the composition of the volcanic precursor, its high concentrations may also be related to hydrothermal alteration and the formation or redistribution of Ba-bearing phases, such as barite ($BaSO_4$). The lack of a clear correspondence between Ba and Sr concentrations suggests that these two elements may have been controlled by different mineralogical or geochemical processes. This contrasts with the Ba–Sr relationship reported for the bentonites from Jebel Ouichane and may indicate differences in the alteration history or in fluid–rock interactions between the two systems (Samaoui et al. 2024 ; Dumańska-Słowik et al. 2021).

The distribution of sulfur and its association with several trace elements provide additional evidence for possible hydrothermal redistribution. Sulfur concentrations increase from 0.02–0.04 wt.% in samples B-S1 to B-S4 to 0.11 wt.% in B-S5. Interestingly, B-S5 also exhibits the highest concentrations of Ba (5,360 ppm), Mn (119 ppm), Cr (35 ppm), Rb (17.4 ppm), Ni (13.6 ppm), Sn (15 ppm), Bi (1.5 ppm), and Mo (2.0 ppm). This concomitant enrichment may indicate a common geochemical control and could be consistent with the involvement of sulfur-bearing hydrothermal fluids.

Sample B-S4 is characterized by a distinct enrichment in Zn (182 ppm), accompanied by relatively elevated concentrations of As (13.7 ppm), Pb (19.3 ppm), Tl (1.55 ppm), and Cu (3.6 ppm). This association differs from the enrichment pattern observed in B-S5 and may reflect localized redistribution of metal-bearing elements during alteration. The coexistence of Zn, As, Pb, and Tl could be compatible with a late hydrothermal overprint involving metal-bearing fluids.

Overall, the trace-element distribution suggests that the geochemical composition of the studied bentonites was influenced not only by the original volcanic material but also by subsequent alteration processes. The contrasting enrichment patterns observed for Ba, sulfur-associated elements, and the Zn–As–Pb–Tl group indicate heterogeneous fluid–rock interaction and may point to more than one stage of hydrothermal alteration (Christidis 1998). In particular, the distinct geochemical signatures of B-S4 and B-S5 could reflect spatially and/or temporally variable hydrothermal conditions, including a relatively late hydrothermal episode associated with the volcanic system.

Table 5. Trace-element concentrations in the analyzed bentonite samples.

Trace element	B-S1	B-S2	B-S3	B-S4	B-S5
Lithophilic elements					
Ba	1350	3560	1140	2040	5360
Be	10.8	12.7	8.4	3.1	9.0
Br	28.8	<0.5	13.3	6.0	8.6
Cs	3.3	3.3	1.7	1.6	4.3
Cr	7	7	8	9	35
Hf	6.3	6.1	5.5	5.2	5.3
Li	4	8	4	3	8
Mn	47	28	11	54	119
Nb	21.5	21.9	19.0	22.3	19.9
Rb	8.8	9.5	7.3	9.5	17.4
Sc	2.1	3.3	2.5	4.3	3.2
Sr	124	135	137	162	163
Ta	1.4	2.1	1.3	1.9	1.9
Th	44	49	46	41	45
U	2.3	2.0	3.6	9.2	2.3
V	15	10	9	22	19
Y	12.7	12.3	10.7	9.6	9.0
Zr	170	161	139	167	139
W	1	<1	<1	<1	<1
Siderophilic elements					
Co	1.1	0.6	0.6	2.5	1.0
Ge	<0.1	<0.1	<0.1	<0.1	<0.1
Ir	<5	<5	<5	<5	<5
Ni	3.6	3.4	4.3	3.7	13.6
Re	<0.001	<0.001	<0.001	<0.001	<0.001
Sn	5	5	4	4	15
Chalcophilic elements					
Ag	0.29	0.30	0.27	0.28	0.26

As	<0.5	1.1	1.5	13.7	2.7
Bi	0.2	0.3	0.2	0.3	1.5
Cd	<0.1	<0.1	<0.1	<0.1	<0.1
Cu	1.9	0.7	0.8	3.6	0.8
Ga	11.8	<0.1	14.5	<0.1	73.9
Hg	<1	<1	<1	<1	<1
In	<0.1	<0.1	<0.1	<0.1	<0.1
Mo	0.7	0.6	0.6	1.4	2.0
Pb	9.4	11.9	14.6	19.3	7.7
Sb	<0.1	0.3	<0.1	0.9	0.3
Se	<0.1	<0.1	<0.1	<0.1	<0.1
Te	<0.1	<0.1	<0.1	<0.1	<0.1
Tl	0.21	0.25	0.20	1.55	0.68
Zn	21.4	<0.5	54.7	182.0	<0.5
S [%]	0.03	0.04	0.02	0.04	0.11

Note: Values preceded by "<" are below the corresponding analytical detection limits. All concentrations are reported in ppm.

8- Geochemical Relationships and Distribution Patterns

Principal component analysis (PCA) was performed to investigate the relationships between trace elements and the geochemical variability of the five bentonite samples (**Figure 14**). The first two principal components, Dim1 and Dim2, explain 39.4% and 37.8% of the total variance, respectively, accounting for 77.2% of the overall variability. This cumulative percentage indicates that the factorial plane provides a useful representation of the main geochemical patterns within the dataset.

Dim1 primarily separates samples B-S1, B-S2, and B-S3, located on the negative side of the axis, from B-S4 and B-S5, positioned on the positive side. Samples B-S1 to B-S3 exhibit directional affinities with Y, W, Hf, Be, and Br, suggesting similarities in their multielement geochemical patterns. In contrast, B-S4 and B-S5 display distinct geochemical signatures, further differentiated along Dim2. B-S5 plots in the upper part of the factorial plane and shows directional affinities with Ba, Cr, Rb, Ni, Sn, and Bi. This pattern is consistent with the concentration data, which identify B-S5 as the most enriched sample in these elements. Conversely, B-S4 is located in the lower-right quadrant and exhibits directional affinities with Zn, As, Pb, Cu, Tl, and U, in agreement with its distinctive trace-element signature, particularly its elevated Zn, As, Pb, and Tl concentrations.

The distribution of the elements classified as lithophile, siderophile, and chalcophile provides an additional framework for examining their geochemical relationships. Overall, the PCA

highlights substantial geochemical heterogeneity among the studied bentonites, particularly the contrasting multielement patterns of B-S4 and B-S5. These differences may reflect variations in the original volcanic material, mineralogical composition, accessory mineral assemblages, and subsequent alteration processes.

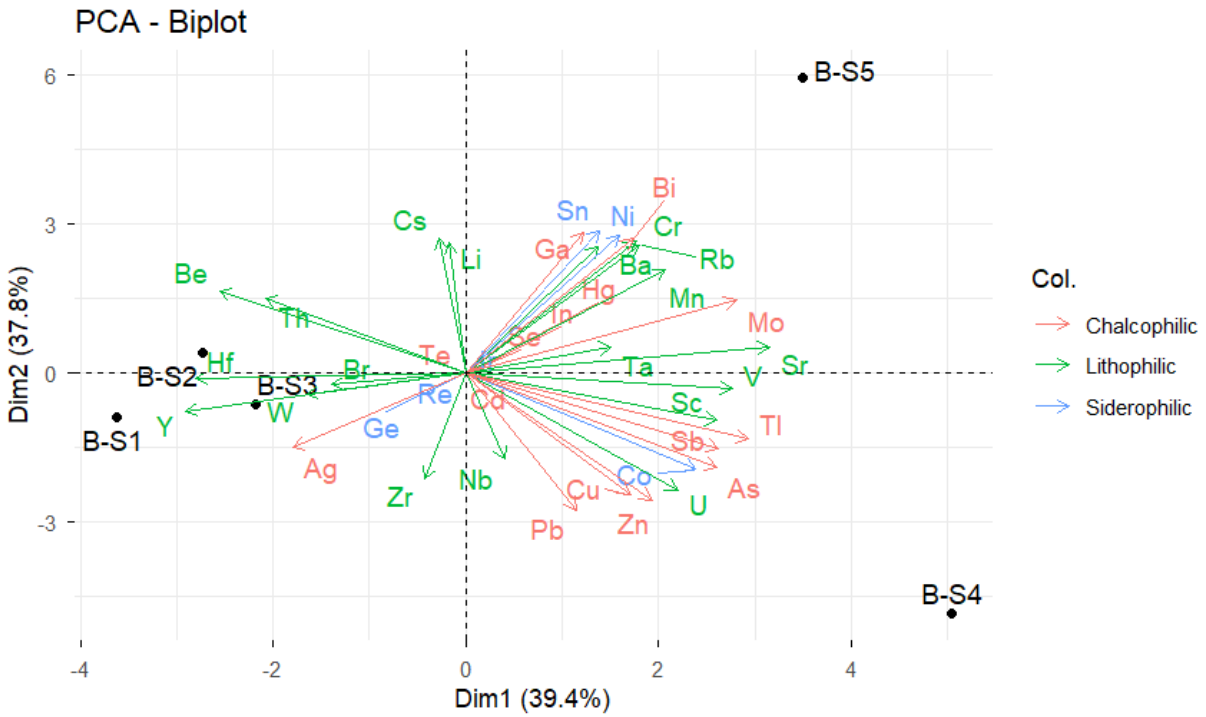


Figure 14. Principal Component Analysis (PCA) of Trace Elements in Bentonite Samples: Geochemical Relationships and Distribution Patterns.

9. Implications for Soda Ash Activation and Potential Industrial Applications

9.1 Calculated Soda Ash Requirements for Bentonite Activation

The calculated soda ash requirements varied among the five bentonite samples according to their cation exchange capacities and cation compositions (**Table 6**). The CEC values ranged from 67 to 103 cmolc/kg, whereas the total concentrations of divalent cations ranged from 49 to 82 cmolc/kg. Exchangeable sodium contents ranged from 23 to 40 cmolc/kg.

The calculated Na_2CO_3 requirements based on divalent cation concentrations ranged from 2.6 to 4.3 wt.%, while those calculated using the CEC-based approach at an activation degree of 110% ranged from 2.5 to 4.2 wt.%. The highest calculated requirement was obtained for sample

B-S1 using the divalent-cation approach (4.3 wt.%), whereas the lowest was obtained for sample B-S5 using the CEC-based approach (2.5 wt.%).

These differences highlight the importance of considering both the exchange capacity and the divalent cation content when estimating the soda ash requirement. The appropriate dosage can be selected by comparing the two estimates for each sample, provided that the calculation methods and the selection criterion are clearly defined.

Table 6. Comparative calculation of soda ash requirements for bentonite activation using the divalent-cation and CEC-based approaches.

Sample	CEC (cmolc/kg)	Total divalent cations (cmolc/kg)	Exchangeable Na^+ (cmolc/kg)	Na_2CO_3 based on divalent cations (wt.%)	Na_2CO_3 based on CEC at 110% activation (wt.%)
B-S1	103	82	40	4.3	3.9
B-S2	94	74	23	3.9	4.2
B-S3	92	67	36	3.6	3.4
B-S4	83	62	27	3.3	3.4
B-S5	67	49	37	2.6	2.5

Note: CEC, cation exchange capacity; wt.%, mass percentage of Na_2CO_3 relative to the dry mass of bentonite. The CEC-based approach assumes an activation degree of 110%.

9.2 Comparative Assessment of Soda Ash Requirements for Bentonite Activation

The comparison between the two calculation approaches highlights the influence of the chemical parameters considered when estimating soda ash requirements for bentonite activation. The CEC-based approach estimates the sodium carbonate requirement from the exchange capacity not compensated by exchangeable sodium, whereas the divalent-cation-based approach considers the stoichiometric demand associated with the precipitation of Ca^{2+} and Mg^{2+} as carbonates. The calculated Na_2CO_3 dosages vary among the five bentonite samples, with the divalent-cation-based approach generally yielding higher values than the CEC-based approach, except for samples B-S2 and B-S4 (**Figure 15**). These differences reflect the distinct

principles underlying the two methods and emphasize the importance of considering both cation exchange properties and divalent cation content when estimating soda ash requirements. Selecting the higher calculated dosage for each sample provides a conservative theoretical estimate of the Na_2CO_3 requirement, although experimental validation is necessary to determine the optimal dosage for effective bentonite activation.

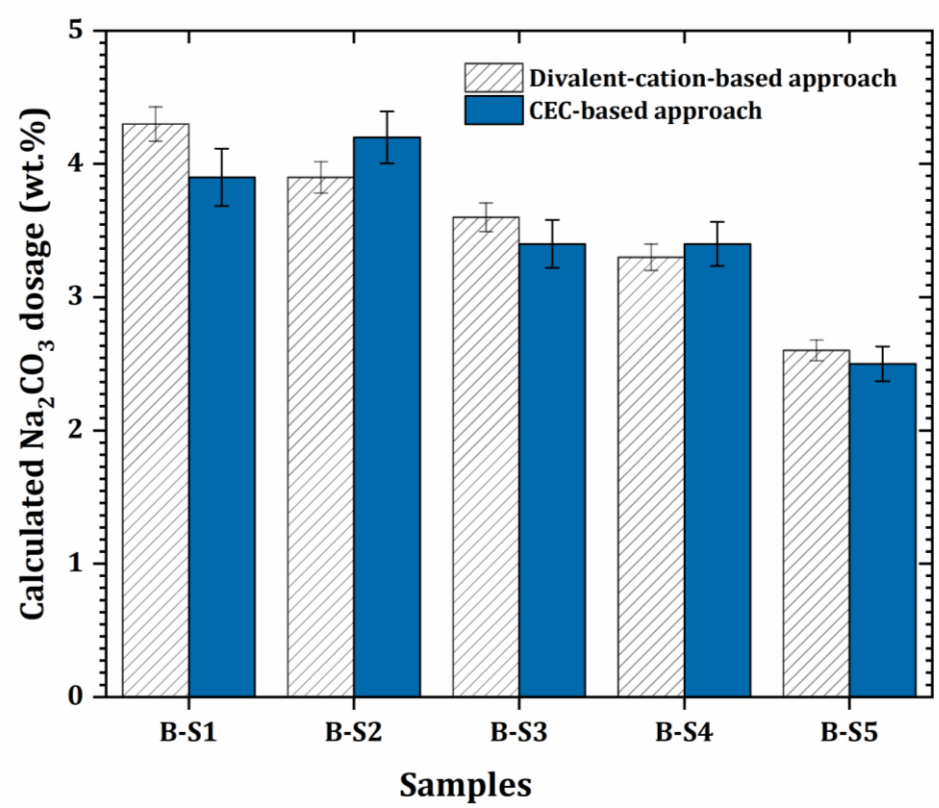


Figure 15. Comparison of calculated Na_2CO_3 dosages for bentonite activation using two approaches.

Figure 16 shows a strong positive linear association between CEC and the calculated Na_2CO_3 dosage derived from the divalent-cation-based approach ($R^2 = 0.984$). This trend indicates that bentonite samples with higher CEC values generally exhibit higher calculated soda ash requirements. However, this association does not establish a causal relationship between CEC and the calculated dosage. The relationship obtained using the CEC-based approach should be examined separately, as CEC is itself a parameter involved in the dosage calculation.

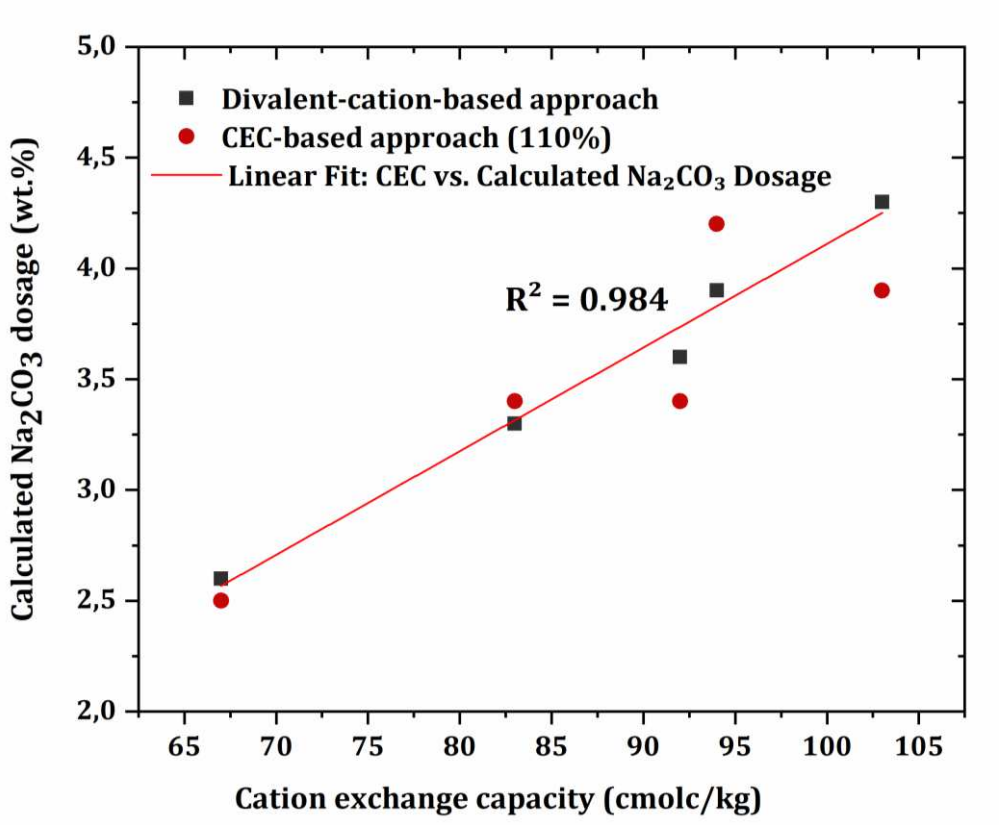
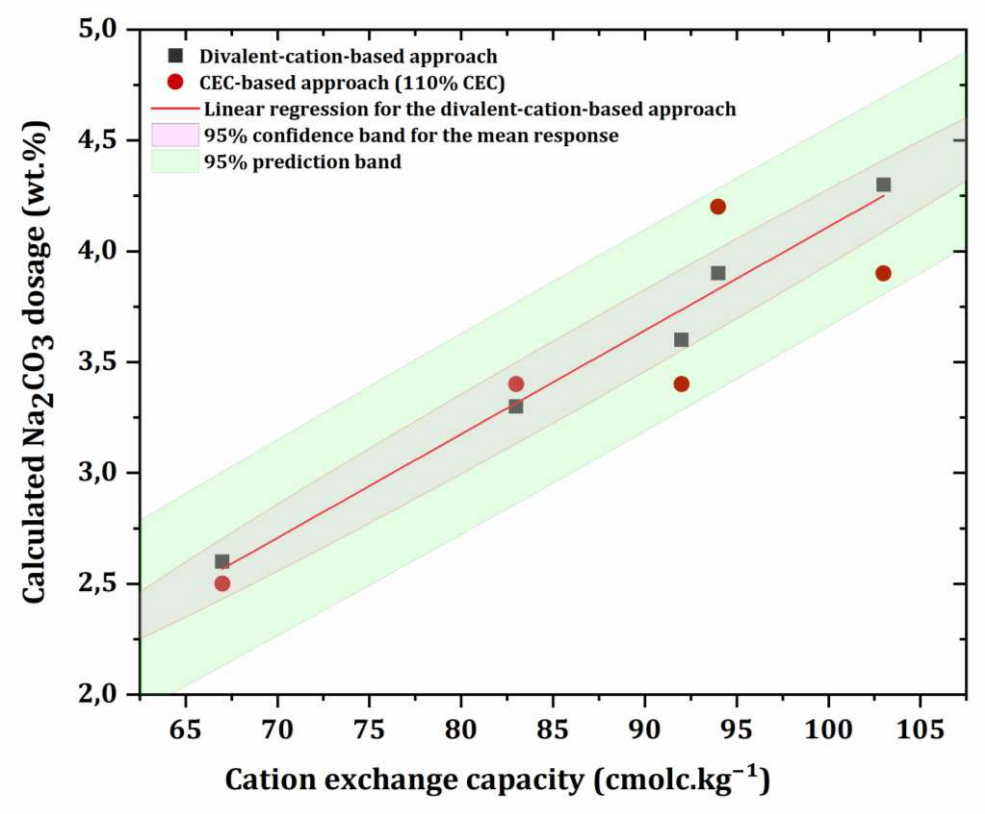


Figure 16. Relationship between cation exchange capacity (CEC) and the calculated Na_2CO_3 dosage using the divalent-cation-based approach (R^2 = 0.984).

The linear regression analysis revealed a strong positive relationship between CEC and the Na_2CO_3 dosage calculated using the divalent-cation-based approach (R^2 = 0.9836). This trend indicates that bentonite samples with higher CEC values tend to require higher calculated soda ash dosages according to this approach (**Figure 17**). The 95% confidence band illustrates the uncertainty associated with the estimated regression line. However, given the limited number of samples (n = 5), this relationship should be interpreted cautiously. The comparison between the two approaches also highlights differences in the calculated Na_2CO_3 requirements, reflecting the distinct parameters considered in each calculation method.



745

746 ***Figure 17.*** *Comparison of Na_2CO_3 dosages calculated using the divalent-cation-based and*
747 *CEC-based approaches for the five bentonite samples. The solid line represents the linear*
748 *regression between CEC and the dosage calculated using the divalent-cation-based approach.*
749 *The shaded area represents the 95% confidence band for the mean response (R^2 = 0.9836).*

750

751 ## V- Discussion

752 The integrated characterization of the five bentonite samples collected from the eastern part of
753 the Jbel Tidienn area reveals a smectite-dominated mineralogical assemblage associated with
754 significant variations in physicochemical, granulometric, and geochemical properties. Smectite
755 contents ranging from 58 to nearly 89 wt.% are consistent with the relatively high cation
756 exchange capacity (CEC) measured in the samples. The FTIR spectra further support the
757 presence of smectitic minerals, particularly montmorillonite, as indicated by characteristic
758 bands associated with structural hydroxyl and silicate vibrations. The basal spacing of
759 approximately 15.5 Å observed by XRD is consistent with hydrated smectite and may indicate
760 the presence of hydrated interlayer cations, although this value alone does not establish their
761 identity. The granulometric results also highlight the textural heterogeneity of the studied
762 bentonites. The predominance of silt-sized particles, together with variations in median grain

diameter (D50) and particle-size dispersion, indicates differences in particle-size distribution that may influence hydration, dispersion, and subsequent processing behavior. These textural variations should therefore be considered alongside the mineralogical and physicochemical characteristics of the materials (El Halim et al. 2025 ; Baković et al. 2026 ; Ait Hmeid et al. 2025a).

Despite the predominance of smectite, the presence of accessory minerals, including quartz/cristobalite, feldspars, illite/mica, zeolite, and calcite, indicates that the studied materials are mineralogically heterogeneous. These phases may influence the bulk chemical composition and the proportion of the material contributing directly to cation exchange. In particular, carbonate-bearing phases should be considered when estimating soda ash requirements. However, the total carbonate content alone is insufficient to determine the optimal Na_2CO_3 dosage, which also depends on the CEC, the initial exchangeable-cation composition, and the activation conditions. Sodium carbonate can promote the replacement of divalent interlayer cations by Na^+ and, under suitable conditions, the precipitation of dissolved Ca^{2+} and Mg^{2+} as carbonates. The extent of these processes depends on the chemical composition of the bentonite and the conditions under which activation is performed (Ait Hmeid et al. 2025b ; Xie et al. 2026 ; Radulović et al. 2026 ; Zhang et al. 2026).

The physicochemical properties also show appreciable variability among the five samples. The alkaline pH values (8.2–9.0) and relatively high CEC values support further investigation of their potential as industrial clay materials. However, the electrical conductivity values, ranging from 176 to 1229 $\mu S\ cm^{-1}$, indicate differences in soluble-ion content. The strong positive relationship between electrical conductivity and NaCl-equivalent content ($R^2 = 0.921$) supports the interpretation that soluble salts contribute substantially to the observed conductivity variation (Kaufhold et al. 2015 ; Chen et al. 2025). Nevertheless, electrical conductivity reflects the overall contribution of dissolved ions and other electrical properties of the suspension; it does not directly quantify the exchangeable sodium content (Christidis et al. 2023). Consequently, conductivity alone cannot be used to determine the Na_2CO_3 requirement, which depends on the exchange capacity, the initial cationic composition, and the assumptions adopted in the dosage calculation (Hosseini et al. 2026).

The major- and trace-element compositions further confirm the geochemical variability of the bentonites despite their occurrence within the same volcanic-sedimentary setting. The relatively high Al_2O_3 contents are consistent with their aluminosilicate-rich composition, whereas

795 variations in SiO_2, alkali oxides, MgO, and CaO reflect differences in bulk chemical
796 composition and potentially in the proportions of the constituent mineral phases. The trace-
797 element data distinguish B-S4 and B-S5 from the other samples. B-S5 is characterized by
798 enrichment in Ba, Mn, Cr, Rb, Ni, Sn, and Bi, whereas B-S4 exhibits comparatively high Zn,
799 As, Pb, and Tl concentrations. These contrasting geochemical signatures may reflect differences
800 in the composition of the original volcanic material, accessory mineral assemblages, and
801 subsequent alteration processes. However, identifying the specific sources of these elements
802 would require additional mineralogical and geochemical evidence (Christidis and Dunham
803 1993 ; Christidis and Huff 2009 ; Ait Hmeid et al. 2021b).

804 The mineralogical, physicochemical, granulometric, and geochemical characterization provides
805 a basis for estimating the Na_2CO_3 requirements of the five bentonites. The samples should not
806 be considered equivalent for activation purposes because their initial cationic compositions and
807 physicochemical properties differ. Two complementary approaches were therefore used to
808 estimate the theoretical soda ash requirement. The first approach is based on the difference
809 between the CEC and the initial exchangeable sodium content, using a target activation degree
810 of 110%. Its main objective is to estimate the sodium requirement for saturating the smectite
811 exchange sites while accounting for the sodium already present in the exchange complex.
812 However, this approach does not explicitly quantify the potential contribution of soluble and
813 exchangeable divalent cations to the overall Na_2CO_3 requirement.

814 The second approach estimates the Na_2CO_3 requirement from the combined concentrations of
815 soluble and exchangeable Ca^{2+} and Mg^{2+}, assuming that these ions can contribute to carbonate
816 precipitation under the activation conditions. Its main objective is to estimate the carbonate
817 requirement associated with the potential removal of divalent cations that may compete with
818 Na^+ during activation. Nevertheless, soluble and exchangeable cations may behave differently
819 because of differences in solution chemistry, mineral dissolution, precipitation, and ion-
820 exchange equilibria. In addition, the extent to which exchangeable cations become available for
821 precipitation cannot be assumed to be complete under all treatment conditions. Consequently,
822 this approach provides a theoretical estimate rather than a direct measurement of Na_2CO_3
823 consumption during activation.

824 The measured cationic composition provides further insight into the differences among the
825 investigated bentonites (Table 3). The total measured cationic charge (ΣCat.) ranged from 90.0
826 to 131.0 cmolc kg^{-1}, with the highest value recorded for B-S1 and the lowest for B-S5.

Magnesium and calcium were the predominant divalent cations, with concentrations ranging from 28.0 to 46.0 cmolc kg^{-1} and from 20.0 to 35.0 cmolc kg^{-1}, respectively. Sodium concentrations varied from 24.0 cmolc kg^{-1} in B-S2 to 46.0 cmolc kg^{-1} in B-S1, whereas potassium concentrations remained relatively low (1.4–3.3 cmolc kg^{-1}). Barium was detected only at trace levels. These variations indicate differences in the measured ionic composition and potentially reflect differences in the contributions of exchangeable cations and soluble salts. However, the relative contributions of these fractions must be interpreted in light of the analytical procedures used to determine them.

Soluble chloride concentrations ranged from 0.6 to 6.5 cmolc kg^{-1}, with B-S1 exhibiting the highest value. The calculated NaCl equivalent also reached its maximum in B-S1 (6.50), compared with values ranging from 0.51 to 2.57 for the other samples. This result suggests a greater contribution of soluble chloride salts in B-S1, although the NaCl equivalent expresses the measured salt content on a sodium chloride basis and does not demonstrate that all the salts are present as NaCl. Chloride alone cannot account for the complete ionic composition, and other anions, including carbonates, bicarbonates, and sulfates, may contribute to charge balance. Their respective contributions would need to be confirmed by direct anion measurements. These results provide additional context for interpreting the behavior of the bentonites in aqueous media and their potential response to soda activation.

The calculated Na_2CO_3 dosages ranged from 2.5 to 4.2 wt.% using the CEC-based approach and from 2.6 to 4.3 wt.% using the divalent-cation-based approach. The two methods did not exhibit a consistent directional difference across all samples: the divalent-cation-based dosage was higher for B-S1 and B-S3, whereas the CEC-based dosage was higher for B-S2 and B-S4. For B-S5, the estimates were similar (2.6 and 2.5 wt.%, respectively). These differences may be related to variations in the relative contributions of exchangeable sodium and divalent cations, as well as the assumptions underlying each calculation method. For example, B-S1 exhibited both the highest sodium concentration (46.0 cmolc kg^{-1}) and the highest combined calcium and magnesium concentration (81.0 cmolc kg^{-1}). This coexistence illustrates that substantial sodium and divalent-cation contributions can occur within the same sample. Accordingly, the estimated soda ash requirement depends on whether the calculation emphasizes the sodium requirement of the exchange complex or the potential carbonate requirement associated with divalent-cation removal.

For preliminary dosage selection, the higher value obtained from the two calculation methods was retained for each sample as a conservative screening criterion. The resulting theoretical dosages were 4.3 wt.% for B-S1, 4.2 wt.% for B-S2, 3.6 wt.% for B-S3, 3.4 wt.% for B-S4, and 2.6 wt.% for B-S5. This selection criterion provides an initial basis for designing sample-specific activation experiments. However, retaining the higher estimate does not guarantee that the selected dosage is optimal, because the two approaches address different theoretical contributions to the activation process and rely on distinct assumptions. The actual Na_2CO_3 requirement may differ because of ion-exchange equilibria, the behavior of soluble and exchangeable cations, mineral dissolution and precipitation reactions, and the specific activation conditions. Moreover, excessive Na_2CO_3 addition may increase the soluble salt content and modify the physicochemical properties of the treated bentonite. Experimental optimization is therefore necessary to identify the dosage that provides the desired activation response while avoiding unnecessary reagent consumption.

A strong positive linear association was observed between CEC and the divalent-cation-based Na_2CO_3 dosage ($R^2 = 0.9836$). This association indicates that the two parameters varied closely across the five samples. However, the relationship should be interpreted cautiously because of the small sample size ($n = 5$) and the dependence of the calculated dosage on the divalent-cation concentrations and the assumptions underlying the calculation method. The high R^2 value does not establish a causal relationship between CEC and Na_2CO_3 requirement, nor does it demonstrate that CEC alone can reliably predict the required dosage. Further validation using experimental activation results and a larger dataset would be necessary to determine whether this relationship has predictive value for bentonites with comparable characteristics.

The observed variability among the samples also has implications for their potential industrial valorization. Their relatively high smectite contents and CEC values suggest that they may be suitable candidates for applications requiring cation exchange, hydration, and swelling properties. Sodium activation could therefore be investigated to improve their suitability for drilling fluids, foundry binders, and other applications requiring appropriate rheological behavior or binding capacity. For drilling-fluid applications, relevant performance indicators include swelling capacity, viscosity, yield behavior, and fluid loss. For foundry applications, binding performance, green compressive strength, and thermal stability would need to be evaluated. Other potential uses, such as adsorption and wastewater treatment, would require application-specific assessment of adsorption capacity, selectivity, and regeneration potential.

These applications remain prospective because the present study characterizes the raw materials and estimates theoretical activation requirements without directly demonstrating the technological performance of the activated products.

Finally, the contrasting trace-element signatures of B-S4 and B-S5 warrant further consideration when evaluating their suitability for specific industrial applications. Although the measured concentrations alone do not establish the presence of environmental risks, the mobility and leachability of relevant elements should be assessed whenever exposure is a concern. Future work should also examine the response of each bentonite to different Na_2CO_3 concentrations and activation conditions, while monitoring changes in exchangeable sodium, CEC, swelling, rheological properties, pH, and soluble salt content. Comparing these experimental results with the two theoretical approaches would help establish whether their combined use improves dosage selection and would provide a stronger basis for evaluating the industrial potential of the studied bentonites.

VI- Conclusions

This study provides an integrated mineralogical, physicochemical, granulometric, and geochemical characterization of five bentonite samples collected from the eastern part of Jbel Tidiennt, within the Neogene Kert Basin in northeastern Morocco. It also compares two complementary approaches for estimating the theoretical sodium carbonate (Na_2CO_3) requirements for bentonite activation.

The results reveal a smectite-dominated mineralogical assemblage, with smectite contents ranging from 58 to nearly 89 wt.%, relatively high cation exchange capacity (CEC), alkaline pH values, and variable proportions of accessory minerals and soluble salts. Differences in soluble and exchangeable cation composition further demonstrate the heterogeneity of the studied materials and highlight the importance of considering the initial chemical characteristics of each bentonite when estimating its activation requirements.

The CEC-based approach, which accounts for the initial exchangeable sodium content and a target activation degree of 110%, yielded theoretical dosages ranging from 2.5 to 4.2 wt.%. The divalent-cation-based approach, which estimates the carbonate requirement associated with the potential precipitation of soluble and exchangeable Ca^{2+} and Mg^{2+}, yielded values ranging from 2.6 to 4.3 wt.%. The differences between the two estimates reflect their distinct calculation principles and assumptions. Selecting the higher value for each sample provides a conservative

preliminary criterion for designing subsequent activation experiments. Nevertheless, these estimates remain theoretical and should not be interpreted as experimentally validated or optimal dosages.

From an industrial perspective, the mineralogical and physicochemical characteristics of the studied bentonites indicate potential for further investigation in applications requiring swelling, cation exchange, rheological control, or binding properties. However, their suitability for specific applications cannot be established from the characterization of the raw materials alone. Experimental validation of the proposed activation dosages and assessment of the technological performance of the activated products are therefore essential steps toward their industrial valorization.

Future research should first focus on systematic laboratory activation tests using Na_2CO_3 concentrations around the calculated values, with controlled variations in treatment conditions. These experiments should quantify actual reagent consumption and evaluate changes in exchangeable sodium content, CEC, swelling capacity, rheological behavior, pH, and soluble salt content. Comparing the experimental results with the predictions of both calculation approaches would help determine their respective accuracy and establish whether their combined use improves dosage optimization.

Subsequent investigations should assess the potential of the activated bentonites for specific industrial applications. For drilling fluids, priority should be given to viscosity, yield behavior, swelling capacity, and fluid-loss measurements. For foundry applications, relevant tests should include green compressive strength, binding performance, and thermal stability. Other potential applications, including adsorption and wastewater treatment, could be explored through tests of adsorption efficiency, selectivity, regeneration capacity, and material stability under operating conditions. Pilot-scale trials, economic assessments, and comparisons with applicable industrial specifications would then be required to evaluate the feasibility of large-scale use.

Finally, further geochemical and environmental investigations should assess the mobility and leachability of selected trace elements, particularly in samples displaying distinct trace-element signatures, such as B-S4 and B-S5. These assessments would help establish the suitability of the materials for applications involving potential environmental exposure.

Overall, this study establishes a preliminary framework for linking bentonite characterization to theoretical soda ash dosage estimation and provides a basis for the experimental optimization and industrial valorization of bentonite resources from northeastern Morocco. Future research

integrating activation efficiency, application-specific performance, environmental compatibility, and economic feasibility will be essential to determine their practical potential for industrial use.

Acknowledgements

The authors gratefully acknowledge the anonymous reviewers for their valuable comments and constructive suggestions, as well as the journal editor for the careful evaluation of the manuscript, which helped enhance its clarity and overall quality.

Author contributions

HAH and AL: Conceptualization, methodology design, software development, resource provision, investigation, validation, and drafting of the original manuscript. SA, MA, GH, ME, CS, AM, AS, KE and ID: Validation, Visualization. All authors have read and approved the final version of the manuscript.

Funding

This research received no funding.

Data availability

The data supporting this study's findings are available from the corresponding author, H. Ait Hmeid upon reasonable request.

Conflict of interest

On behalf of all authors, the corresponding author states that there is no conflict of interest.

References

Aalaoul M, Azdimousa A, El Hammouti K (2015) Bentonite's reserves geometry of Trebia deposit in Nador region (northeastern Morocco): contributions of geophysical surveys and core drilling campaign. Journal of Materials and Environmental Science 6(12):3564–3573.

AFNOR (1996) Sols: reconnaissance et essais — Détermination de la teneur en carbonate — Méthode du calcimètre. Standard NF P 94-048. Association Française de Normalisation, Paris, France.

Ait Hmeid H, Akodad M, Aalaoul M, Baghour M, Moumen A, Skalli A, Anjjar A, Conti P, Sfalanga A, Khyabani FR, Minucci S, Daoudi L (2021a) Clay mineralogy, chemical and geotechnical characterization of bentonite from Beni Bou Ifrour Massif (the Eastern Rif, Morocco). Geol Soc Spec Publ 502:31–44. https://doi.org/10.1144/SP502-2019-25.

Ait Hmeid H, Akodad M, Aalaoul M, Baghour M, Moumen A, Skalli A, Daoudi L (2019) Particle size distribution and statistical analysis of the grain size of Messinian bentonite from the Kert Basin (northern Morocco). Materials Today: Proceedings 13:505–514. https://doi.org/10.1016/j.matpr.2019.04.007.

Ait Hmeid H, Akodad M, Baghour M, Moumen A, Skalli A, Azizi G, Gueddari H, Maach M, Aalaoul M, Anjjar A, Daoudi L (2021b) Valorization of Moroccan bentonite deposits: "Purification and treatment of margin by the adsorption process". Molecules 26(18):5528. https://doi.org/10.3390/molecules26185528.

Ait Hmeid H, Akodad M, El Halim M, Omdi FE, Baghour M, Skalli A, Sadik C, Aalaoul M, Ikirri M, Abioui M, Maach M, Chahban M, Daoudi L (2025a) Assessment of bentonite effectiveness in retaining pollutants from olive oil production discharges. Interactions 246:49. https://doi.org/10.1007/s10751-025-02263-2.

Ait Hmeid H, Akodad M, El Halim M, Omdi FE, Baghour M, Skalli A et al (2025b) Comparative analysis of Na+ and Ca2+ ion effects on the physical-chemical properties of bentonite: implications for industrial applications. Ore Energy Res Geol 18:100095. https://doi.org/10.1016/j.oreoa.2025.100095.

Ammann L (2003) Cation exchange and adsorption on clays and clay minerals. Thesis, University of Kiel, Germany.

Ammann L, Bergaya F, Lagaly G (2005) Determination of the cation exchange capacity of clays with copper complexes revisited. Clay Minerals 40(4):441–453. https://doi.org/10.1180/0009855054040182.

Arslan M, Abdioğlu E, Kadir S (2010) Mineralogy, geochemistry, and origin of bentonite in Upper Cretaceous pyroclastic units of the Tirebolu area, Giresun, northeast Turkey. Clays Clay Miner 58:120–141. https://doi.org/10.1346/CCMN.2010.0580112.

ASTM Committee D-18 on Soil and Rock (2017) Standard practice for classification of soils for engineering purposes (Unified Soil Classification System). ASTM International.

Azdimousa A, Jabaloy A, Asebriy L, Booth-Rea G, González-Lodeiro F, Bourgois J (2007) Lithostratigraphy and structure of the Temsamane unit (eastern external Rif, Morocco). Rev Soc Geol Esp 20(3–4):187–200.

Babiy S, Tuttolomondo A, Laloui L (2025) Experimental quantification of capillary and adsorbed water in active clays for hydro-mechanical modelling. Can Geotech J 62:1–18. https://doi.org/10.1139/cgj-2025-0323.

Bahranowski C, Klimek A, Gaweł A, Bąk J, Zimowska M, Wójcik-Bania M, et al (2021) Rehydration driven Na-activation of bentonite—evolution of the clay structure and composition. Materials 14:7622. https://doi.org/10.3390/ma14247622.

Baković T, Robisson A, Preinstorfer P, Liberto T (2026) Understanding the high variability of clays: a rheological approach. Mater Struct 59:158.

Barcos L, Jabaloy A, Azdimousa A, Asebriy L, Gómez-Ortiz D, Rodríguez-Peces MJ, et al (2014) Study of relief changes related to active doming in the eastern Moroccan Rif (Morocco) using geomorphological indices. J Afr Earth Sci 100:493–509. https://doi.org/10.1016/j.jafrearsci.2014.07.014.

Belghazdis M, El-Kaber H, Bendouch A (2022) Natural clays from Morocco: potentials and applications. J Sustain Sci Manag 17(2):240–254.

Belousov PE, Karelina ND (2022) Volcano-sedimentary and hydrothermal bentonite deposits. J Volcanol Seismol 16:451–461. https://doi.org/10.1134/S0742046322060021.

Benhammou A, Tanouti B, Nibou L, Yaacoubi A, Bonnet JP (2009) Mineralogical and physicochemical investigation of Mg-smectite from Jbel Ghassoul, Morocco. Clays Clay Miner 57:264–270. https://doi.org/10.1346/CCMN.2009.0570212.

Bish DL, Duffy CJ (1990) Thermogravimetric analysis of minerals. In: Stucki JW, Bish DL, Mumpton FA (eds) Thermal analysis in clay science. CMS Workshop Lectures, vol 3. The Clay Minerals Society. https://doi.org/10.1346/CMS-WLS-3.4.

Bishop J, Murad E, Dyar MD (2002) The influence of octahedral and tetrahedral cation substitution on the structure of smectites and serpentines as observed through infrared spectroscopy. Clay Minerals 37(4):617–628. https://doi.org/10.1180/0009855023740064.

Bradbury MH, Baeyens B (2003) Porewater chemistry in compacted re-saturated MX-80 bentonite. Journal of Contaminant Hydrology 61(1–4):329–338. https://doi.org/10.1016/S0169-7722(02)00125-0.

Cao B, Xu J, Wang F, Zhang Y, O'Connor D (2021) Vertical barriers for land contamination containment: a review. Int J Environ Res Public Health 18:12643. https://doi.org/10.3390/ijerph182312643.

Carroll D (1959) Ion exchange in clays and other minerals. Geological Society of America Bulletin 70(6):749–780. https://doi.org/10.1130/0016-7606(1959)70[749:IEICAO]2.0.CO;2.

Chalouan A, Galindo-Zaldívar J, Akil M, Marín C, Chabli A, Ruano P, et al (2006) Tectonic wedge escape in the southwestern front of the Rif Cordillera (Morocco). In: Tectonics of the Western Mediterranean and North Africa. Geological Society, London, Special Publications 262. https://doi.org/10.1144/GSL.SP.2006.262.

Charkaoui H, Azdem D, Mabrouki J, El Hajjaji S (2025) Moroccan bentonite as a sustainable adsorbent: preparation, purification, Na-activation, and structure–property relationships for organic pollutant remediation. ChemistrySelect 10(42):e04647. https://doi.org/10.1002/slct.202504647.

Chen H, Chou C, Peruzzo L, Borglin S, Chang C, Bandai T, Kneafsey T, Nakagawa S, Birkholzer J, Zheng L, Wu Y (2025) Development of an ERT-based framework for bentonite buffers monitoring from laboratory tests: 1. Characterizing thermal–hydrological–mechanical processes. J Geophys Res Solid Earth 130(8):e2024JB030798. https://doi.org/10.1029/2024JB030798.

Christidis G (1998) Comparative study of the mobility of major and trace elements during alteration of an andesite and a rhyolite to bentonite, in the islands of Milos and Kimolos, Aegean, Greece. Clays Clay Miner 46:379–399. https://doi.org/10.1346/CCMN.1998.0460403

Christidis GE, Chryssikos GD, Derkowski A, Dohrmann R, Eberl DD, Joussein E, Kaufhold S (2023) Methods for determination of the layer charge of smectites: a critical assessment of existing approaches. Clays Clay Miner 71:25–53. https://doi.org/10.1007/s42860-023-00234-8

Christidis GE, Dunham AC (1993) Compositional variations in smectites: Part I. Alteration of intermediate volcanic rocks. A case study from Milos Island, Greece. Clay Miner 28:255–273. https://doi.org/10.1180/claymin.1993.028.2.07.

Christidis GE, Huff WD (2009) Geological aspects and genesis of bentonites. Elements 5:93–98. https://doi.org/10.2113/gselements.5.2.93.

Davarpanah SM, Narimani S, Sharghi M, Vásárhelyi B (2025) Introducing coefficients of curvature (Cc) and uniformity (Cu) based on RQD for rock mass characterization. Rock Mechanics Letters 2(1):76–78. https://doi.org/10.70425/rml.202501.10.

Davis CW, Vacher HC (1940) Bentonite: its properties, mining, preparation, and utilization. US Geological Survey Bulletin 609. US Government Printing Office, Washington, DC.

Ddani M, Meunier A, Zahraoui M, Beaufort D, El Wartiti M, Fontaine C, Boukili B, El Mahi B (2005) Clay mineralogy and chemical composition of bentonites from the Gourougou

volcanic massif (northeast Morocco). Clays and Clay Minerals 53(3):250–267. https://doi.org/10.1346/CCMN.2005.0530305.

Delavernhe L, Steudel A, Darbha GK, Schäfer T, Schuhmann R, Wöll C, Geckeis H, Emmerich K (2015) Influence of mineralogical and morphological properties on the cation exchange behavior of dioctahedral smectites. Colloids and Surfaces A: Physicochemical and Engineering Aspects 481:591–599. https://doi.org/10.1016/j.colsurfa.2015.05.031.

Derkowski A, Drits VA, McCarty DK (2012) Nature of rehydroxylation in dioctahedral 2:1 layer clay minerals. Am Mineral 97:610–629. https://doi.org/10.2138/am.2012.3871.

Derkowski A, Kuligiewicz A (2022) Thermal analysis and thermal reactions of smectites: a review of methodology, mechanisms, and kinetics. Clays Clay Miner 70:946–972. https://doi.org/10.1007/s42860-023-00222-y.

Di Emidio G, Verastegui-Flores RD, Mazzieri F, et al (2017) Modified clays for barriers: a review. Innov Infrastruct Solut 2:47. https://doi.org/10.1007/s41062-017-0073-8.

Dixon DA, Hnatiw DSJ, Walker BT (1992) The bentonite industry in North America. Report AECL-10587. Atomic Energy of Canada Limited, Whiteshell Nuclear Research Establishment, Pinawa, Manitoba, Canada.

Dohrmann R, Genske D, Karnland O et al (2012) Interlaboratory CEC and Exchangeable Cation Study of Bentonite Buffer Materials: II. Alternative Methods. Clays Clay Miner 60:176–185. https://doi.org/10.1346/CCMN.2012.0600207.

Dohrmann R, Kaufhold S (2009) Three new, quick CEC methods for determining the amounts of exchangeable calcium cations in calcareous clays. Clays and Clay Minerals 57(3):338–352. https://doi.org/10.1346/CCMN.2009.0570306.

Dumańska-Słowik M, Naglik B, Toboła T, Powolny T, Huber M, Milovska S, Dobosz N, Guzik K (2021) Origin and occurrence of gem-quality, skarn-hosted barite from Jebel Ouichane near Nador in Morocco. Scientific Reports 11:10307. https://doi.org/10.1038/s41598-021-89692-5.

Dumańska-Słowik M, Naglik B, Toboła T, Powolny T, Huber M, Milovska S, Dobosz N, Guzik K (2021) Origin of gem-quality barite at Jebel Ouichane district in Nador, Morocco: implications from integrated fluid inclusions, stable isotopes, and geochemistry. Research Square. https://doi.org/10.21203/rs.3.rs-143678/v1.

Ebrahim SA, Mosaad MM, Othman HA, Hassabo AG (2026) Clay minerals in textile engineering: synthesis, characterization and applications of polymer-clay nanocomposites for enhanced fabric performance. Egypt J Chem 69(3):463–503.

El Bakkali S (1995) Volcanologie et magmatologie du système du Gourougou (Rif nord-oriental, Maroc). PhD thesis, Université de Clermont-Ferrand, France, 256 p.

El Bakkali S, Bourdier JL, Gourgaud A, Vincent PM, El Amrani Hassani I, El Mouraouah AE (2001) Résurgence caldeirique au Miocène supérieur et origine du gisement de fer de Nador (Rif nord-oriental, Maroc). In: Deuxième Colloque international sur le magmatisme, le métamorphisme et les minéralisations associées (3MA), Marrakech, Maroc, 87 p.

El Bakkali S, Gourgaud A, Bourdier JL, Bellon H, Gundogdu N (1998) Post-collision Neogene volcanism of the Eastern Rif (Morocco): magmatic evolution through time. Lithos 45:523–543. https://doi.org/10.1016/S0024-4937(98)00048-6.

El Farricha S (2022) Fabrication d'agrégats à partir de déchets : recherche sur l'incorporation d'argiles réactives dans des matériaux dédiés aux filières de construction de sol. Dissertation, Université de Limoges.

El Halim M, Daoudi L, El Boudour El Idrissi H, El Ouahabi M, Omdi FE, Gourfi A, Ait Hmeid H, Id Abdellah H, Fagel N (2025) Combination of physico-chemical and lead isotope analyses for the provenance study of the archaeological materials: example of Saadien ceramics (16th century, Marrakech Morocco). Ceramics 8:13. https://doi.org/10.3390/ceramics8010013

El Miz M, Akichoh H, Berraaouan D, Salhi S, Tahani A (2017) Chemical and physical characterization of Moroccan bentonite taken from Nador (north of Morocco). Am J Chem 7(4):105–112.

Et-Tayea Y, Harrati A, Rachid A, Nasri H, Attou A, Arkame Y, Manni A, Mamouch Y, El Bouari A, El Khazanti F, Sadik C (2023) Mineralogical and physico-chemical characterization of bentonite materials from the Oued Zemmour area (Oriental Rif, Nador-Morocco): valorization in ceramic field. Bol Soc Esp Ceram Vidr 62:268–283. https://doi.org/10.1016/j.bsecv.2022.03.001.

Et-Tayea Y, Rachid A, Attou A, Nasri H, Mamouch Y, El Khazanti F, El Azhari H, El Haddar A, Aziz A (2021) A new bentonite deposit prospected in the Cap des Trois Fourches area (north-eastern Rif, Morocco) using spectrometry by satellite imagery coupled with mineralogical, chemical, and microstructural investigations. Arab J Geosci 14:2852. https://doi.org/10.1007/s12517-021-08551-9.

Faure-Muret A, Morel JL, Dahmani M (1994) Carte néotectonique du Maroc. Notes et Mémoires du Service Géologique du Maroc 368.

Ferrage E, Lanson B, Sakharov BA, Geoffroy N, Jacquot E, Drits VA (2007) Investigation of dioctahedral smectite hydration properties by modeling of X-ray diffraction profiles: Influence of layer charge and charge location. American Mineralogist 92:1731–1743. https://doi.org/10.2138/am.2007.227.

Fletcher P, Sposito G (1989) The chemical modelling of clay/electrolyte interactions for montmorillonite. Clay Minerals 24(2):375–391. https://doi.org/10.1180/claymin.1989.024.2.14.

Frinak EK, Mashburn CD, Tolbert MA, Toon OB (2005) Infrared characterization of water uptake by low-temperature Na-montmorillonite: Implications for Earth and Mars. Journal of Geophysical Research: Atmospheres 110:D09308. https://doi.org/10.1029/2004JD005647.

García-Rivas J, Dias MI, Paiva I, Fernandes PG, Marques R, García-Romero E, Suárez M (2025) Mineralogical and geochemical characterization of the Benavila (Portugal) bentonites. Minerals 15:836. https://doi.org/10.3390/min15080836.

García-Romero E, Lorenzo A, García-Vicente A, Morales J, García-Rivas J, Suárez M (2021) On the structural formula of smectites: A review and new data on the influence of exchangeable

cations. Journal of Applied Crystallography 54:251–262. https://doi.org/10.1107/S1600576720016040.

Gilg HA, Kaufhold S, Ufer K (2020) Smectite and bentonite terminology, classification, and genesis. In: Bentonites: characterization, geology, mineralogy, analysis, mining, processing and uses, pp 1–18.

Grim RE (1968) Clay mineralogy, 2nd edn. McGraw-Hill, New York.

Grim RE, Güven N (1978) Bentonites: geology, mineralogy, properties and uses. Developments in Sedimentology, vol 24. Elsevier, Amsterdam, New York.

Guillemin M, Hernandez J, Wildi W (1983) Carte géologique du Rif, échelle 1:50 000, feuille Melilla. Notes et Mémoires du Service Géologique du Maroc 297.

Harvey CC, Lagaly G (2013) Industrial applications. In: Bergaya F, Lagaly G (eds) Handbook of clay science. Developments in Clay Science, vol 5, pp 451–490. Elsevier, Amsterdam.

Heiri O, Lotter AF, Lemcke G (2001) Loss on ignition as a method for estimating organic and carbonate content in sediments: reproducibility and comparability of results. Journal of Paleolimnology 25:101–110. https://doi.org/10.1023/A:1008119611481.

Hernandez J (1983) Le volcanisme Miocène du Rif Oriental (Maroc): géologie, pétrologie et minéralogie d'une province shoshonitique. PhD thesis, Université Pierre et Marie Curie, Paris VI, Paris, France, 592 p.

Hernandez J, Bellon H (1985) K-Ar radiometric chronology of Miocene volcanics in eastern Morocco: tectonic and magmatologic implications. Revue de Géologie Dynamique et de Géographie Physique 26(2):85–94.

Hosterman JW, Patterson SH (1992) Bentonite and Fuller's earth resources of the United States. US Geological Survey Professional Paper 1522. US Government Printing Office, Washington, DC.

Hosseini ST, Azin R, Osfouri S, Mohammadian E (2026) A comprehensive review on bentonite and its applications in petroleum industry. Rev Chem Eng 42(3):249–268.

Huff WD (2016) K-bentonites: a review. Am Mineral 101:43–70. https://doi.org/10.2138/am-2016-533.

Imame S, Houssaini J, Atlas H, Ziyat H, Boukhlifi F (2025) Harnessing natural bentonite as a sustainable adsorbent for efficient removal of basic fuchsin dye from aqueous media. Int J Environ Anal Chem 105(19):8191–8212. https://doi.org/10.1080/03067319.2025.2471406.

ISO (2007) ISO 10304-1:2007. Water quality—Determination of dissolved anions by liquid chromatography of ions—Part 1: Determination of bromide, chloride, fluoride, nitrate, nitrite, phosphate and sulfate. International Organization for Standardization, Geneva.

ISO (2011) DIN EN ISO 12677:2011. Chemical analysis of refractory products by X-ray fluorescence (XRF)-Fused cast-bead method. International Organization for Standardization, Geneva.

ISO (2020) ISO 13320:2020: Particle size analysis—Laser diffraction methods. International Organization for Standardization, Geneva, Switzerland.

ISO 11465 (1999) Soil quality—Determination of dry matter and water content of soil—Gravimetric method. Polish Standard.

Jackson ML (1969) Soil chemical analysis—advanced course, 2nd edn. M.L. Jackson, Madison, Wisconsin, USA.

Karagüzel C, Çetinel T, Boylu F, Çinku K, Çelik MS (2010) Activation of (Na, Ca)-bentonites with soda and MgO and their utilization as drilling mud. Applied Clay Science 48(3):398–404. https://doi.org/10.1016/j.clay.2010.01.01.

Kaufhold S, Dohrmann R, Klinkenberg M, Noell U (2015) Electrical conductivity of bentonites. Appl Clay Sci 114:375–385. https://doi.org/10.1016/j.clay.2015.05.032.

1272 Kogel JE, Lewis SA (2001) Baseline studies of the Clay Minerals Society source clays:
1273 Chemical analysis by inductively coupled plasma-mass spectroscopy (ICP-MS). Clays Clay
1274 Miner 49:387–392.
1275
1276 Kumari N, Mohan C (2021) Basics of clay minerals and their characteristic properties. In: Do
1277 Nascimento GM (ed) Clay and Clay Minerals. IntechOpen, London.
1278 https://doi.org/10.5772/intechopen.97672.
1279 Laine H, Karttunen P (2010) Long-term stability of bentonite: a literature review.
1280
1281 Leblanc D (1979) Étude géologique dans le Rif externe oriental au nord de Taza (Maroc). Notes
1282 et Mémoires du Service Géologique du Maroc 281:160 p.
1283
1284 Li KJ, Kurniawan A, Christidis GE, He JY, Zhou CH (2024) Interfacial interactions controlling
1285 adsorption of metal cations on montmorillonite. Am Mineral 109:633–655.
1286 https://doi.org/10.2138/am-2022-8834.
1287
1288 Lo Dico G, Lisuzzo L, Carcelén V, Cavallaro G, Haranczyk M (2024) Thermogravimetric
1289 analysis of moisture in natural and thermally treated clay materials. Materials 17:2231.
1290 https://doi.org/10.3390/ma17102231.
1291
1292 Loeppert RH, Suarez DL (1996) Carbonate and gypsum. In: Sparks DL (ed) Methods of Soil
1293 Analysis, Part 3: Chemical Methods. Soil Science Society of America, pp 437–474.
1294 https://doi.org/10.2136/sssabookser5.3.c15.
1295
1296 Louaya A, Hamoumi N (2010) Étude morphostructurale de la région de Nador (Maroc nord-
1297 oriental). Africa Geoscience Review 17(2):107–127.
1298
1299 Luckham PF, Rossi S (1999) The colloidal and rheological properties of bentonite suspensions.
1300 Advances in Colloid and Interface Science 82(1–3):43–92. https://doi.org/10.1016/S0001-
1301 8686(99)00005-6.
1302
1303 Macheca AD, Mapossa AB, Cumbane AJ, Sulemane AE, Tichapondwa SM (2022)
1304 Development and characterization of Na_2CO_3-activated Mozambican bentonite: prediction of

optimal activation conditions using statistical design modeling. Minerals 12(9):1116. https://doi.org/10.3390/min12091116.

Madejová J (2003) FTIR techniques in clay mineral studies. Vibrational Spectroscopy 31(1):1–10. https://doi.org/10.1016/S0924-2031(02)00065-6.

Madejová J, Balan E, Petit S (2010) Application of vibrational spectroscopy to the characterization of phyllosilicates and other industrial minerals. In: EMU Notes in Mineralogy, vol 9. https://doi.org/10.1180/EMU-notes.9.6.

Madejová J, Komadel P (2001) Baseline studies of the Clay Minerals Society source clays: Infrared methods. Clays and Clay Minerals 49:410–432. https://doi.org/10.1346/CCMN.2001.0490508.

Mahmoud, M., Mohamed, A., Kamal, M. S., Sultan, A., & Hussein, I. (2019). Upgrading Calcium Bentonite to Sodium Bentonite Using Seawater and Soda Ash. Energy & Fuels, 33(11), 10888–10894. https://doi.org/10.1021/acs.energyfuels.9b02900.

Martín-Martín M, Guerrera F, Hlila R, Maaté A, Maaté S, Tramontana M, et al (2020) Tectono-sedimentary Cenozoic evolution of the El Habt and Ouezzane tectonic units (External Rif, Morocco). Geosciences 10:487. https://doi.org/10.3390/geosciences10120487.

Martín-Martín M, Guerrera F, Maaté A, Hlila R, Serrano F, Cañaveras JC, Paton D, Alcalá FJ, Maaté S, Tramontana M, Martín-Pérez JA (2022) The Cenozoic evolution of the Intrarif (Rif, Morocco). Geosphere 18(2):850–884. https://doi.org/10.1130/GES02199.1.

Michalski JR, Kraft MD, Sharp TG, Christensen PR (2003) Thermal infrared spectroscopy of the silica polymorphs and considerations for remote sensing of Mars. Geophysical Research Letters 30(19):2008. https://doi.org/10.1029/2003GL018354.

Michard A, Frizon de Lamotte D, Negro F, Saddiqi O (2007) Serpentinite slivers and metamorphism in the External Maghrebides: arguments for an intracontinental suture in the African paleomargin (Morocco, Algeria). Revista de la Sociedad Geológica de España 20(3–4):173–186.

Moore DM, Reynolds RC Jr (1989) X-ray diffraction and the identification and analysis of clay minerals. Oxford University Press, Oxford.

Moussout H, Ahlafi H, Aazza M, Chfaira R, Mounir C (2020) Interfacial electrochemical properties of natural Moroccan Ghassoul (stevensite) clay in aqueous suspension. Heliyon 6(3):e03634. https://doi.org/10.1016/j.heliyon.2020.e03634.

Muhammad N, Siddiqua S (2022) Calcium bentonite vs sodium bentonite: the potential of calcium bentonite for soil foundation. Mater Today Proc 48:822–827. https://doi.org/10.1016/j.matpr.2021.02.386.

Münch P, Roger S, Cornée JJ, Saint Martin JP, Féraud G, Moussa AB (2001) Restriction des communications entre l'Atlantique et la Méditerranée au Messinien: apport de la téphrochronologie dans la plate-forme carbonatée et le bassin de Melilla–Nador (Rif nord-oriental, Maroc). C R Acad Sci Ser IIA Earth Planet Sci 332(9):569–576. https://doi.org/10.1016/S1251-8050(01)01578-6.

Murray HH (2006) Applied clay mineralogy: occurrences, processing and applications of kaolins, bentonites, palygorskite-sepiolite, and common clays. Developments in Clay Science, vol 2. Elsevier, Amsterdam.

Nasri H, Azdimousa A, El Hammouti K, El Haddar A, El Ouahabi M (2019) Characterization of Neogene marls from the Kert Basin (northeast Morocco): suitability for the ceramics industry. Clay Miner 54(4):379–392. https://doi.org/10.1180/clm.2019.50.

Önal M (2006) Physicochemical properties of bentonites: an overview. Communications in Soil Science and Plant Analysis 37(15–20):2115–2130.

Patel HA, Somani RS, Bajaj HC, Jasra RV (2006) Nanoclays for polymer nanocomposites, paints, inks, greases and cosmetics formulations, drug delivery vehicle and waste water treatment. Bull Mater Sci 29:133–145. https://doi.org/10.1007/BF02704606.

Plevova E, Vaculikova L, Valovicova V (2020) Thermal analysis and FT-IR spectroscopy of synthetic clay mineral mixtures. Journal of Thermal Analysis and Calorimetry 142:507–518. https://doi.org/10.1007/s10973-020-09527-9.

Pret D (2003) Nouvelles méthodes quantitatives de cartographie de la minéralogie et de la porosité dans les matériaux argileux: application aux bentonites compactées des barrières ouvragées. Dissertation, CEA, Grenoble.

Rachidi M, Adil S, Belkasmi M, Sadequi M (2024) Petrographic, mineralogical and geochemical characterization of the Tidiennit volcanic complex (eastern Rif). BIO Web Conf 115:05001. https://doi.org/10.1051/bioconf/202411505001.

Rachidi M, Adil S, Belkasmi M, Sadequi M (2024) Petrographic, mineralogical and geochemical characterization of the Tidiennit volcanic complex (eastern Rif). BIO Web of Conferences 115:05001. https://doi.org/10.1051/bioconf/202411505001.

Radulović D, Stojanović J, Marković M, Todorović D, Jovanović V, Terzić A (2026) Alkali activation of natural calcium bentonite for foundry applications: structural, physicochemical, and technological characterization. Materials 19:2822. https://doi.org/10.3390/ma19132822.

Randhawa KS (2024) Synthesis, properties, and environmental impact of hybrid pigments. The Scientific World Journal 2024:2773950. https://doi.org/10.1155/tswj/2773950.

Reid-Soukup DA, Ulery AL (2002) Smectites. In: Dixon JB, Schulze DG (eds) Soil mineralogy with environmental applications. SSSA Book Series 7, pp 467–499. https://doi.org/10.2136/sssabookser7.c15.

Ross CS, Shannon EV (1926) The minerals of bentonite and related clays and their physical properties. J Am Ceram Soc 9:77–96. https://doi.org/10.1111/j.1151-2916.1926.tb18305.x.

Ross DS, Ketterings Q (2011) Recommended methods for determining soil cation exchange capacity. In: Recommended Soil Testing Procedures for the Northeastern United States, 3rd edn. Northeast Regional Publication No. 493.

Samaoui S, Aabi A, Boushaba A, Mohammed B, Nait Bba A, Essaifi A, Baidder L, Lamrani O (2024) Metallogeny and genesis of fault-filling barite-sulfide veins (Ougnat, Morocco): petrography, fluid inclusion, and Sr-S isotopic constraints. Geosciences 14:83. https://doi.org/10.3390/geosciences14030083.

Saxton KE, Rawls WJ (2006) Soil water characteristic estimates by texture and organic matter for hydrologic solutions. Soil Science Society of America Journal 70(5):1569–1578. https://doi.org/10.2136/sssaj2005.0117.

Seidi A, Benhamou M, Khalil D, Aalaoul M, Bennani MN (2024) Elaboration and characterization of a natural bentonite-poly (ethylene glycol) composite: Development of an exact theoretical study in function of the polymer-density. Chemical Physics Impact 9:100673. https://doi.org/10.1016/j.chphi.2024.100673.

Shepard FP (1954) Nomenclature based on sand–silt–clay ratios. Journal of Sedimentary Research 24:151–158. https://doi.org/10.1306/D4269774-2B26-11D7-8648000102C1865D.

Sposito G (1989) Surface reactions in natural aqueous colloidal systems. Chimia 43(6):169. https://doi.org/10.2533/chimia.1989.169.

Sutherland WM (2024) Wyoming bentonite—Summary report.

Suter G (1965) La région du Moyen Ouerrha (Rif, Maroc): étude préliminaire sur la tectonique et la stratigraphie. Notes et Mémoires du Service Géologique du Maroc 24:7–17.

U.S. EPA (1994) Method 200.7: Determination of metals and trace elements in water and wastes by inductively coupled plasma-atomic emission spectrometry, Revision 4.4. U.S. Environmental Protection Agency, Cincinnati, OH.

U.S. EPA (1996) Method 3052: Microwave assisted acid digestion of siliceous and organically based matrices. U.S. Environmental Protection Agency, Washington, DC.

U.S. Geological Survey (2001) A laboratory manual for X-ray powder diffraction: Smectite group. U.S. Geological Survey. https://pubs.usgs.gov/of/2001/of01-041/htmldocs/clays/smc.htm.

Vantelon D, Pelletier M, Michot LJ, Barrès O, Thomas F (2001) Fe, Mg and Al distribution in the octahedral sheet of montmorillonites: An infrared study in the OH-bending region. Clay Minerals 36(3):369–379. https://doi.org/10.1346/CCMN.2001.0490508.

Wentworth CK (1922) A scale of grade and class terms for clastic sediments. The Journal of Geology 30(5):377–392. https://doi.org/10.1086/62291.

Wilson J, Cressey G, Cressey B, Cuadros J, Ragnarsdottir KV, Savage D, Shibata M (2006) The effect of iron on montmorillonite stability. (II) Experimental investigation. Geochim Cosmochim Acta 70:323–336. https://doi.org/10.1016/j.gca.2005.09.023.

Xi Y, Ding Z, He H, Frost RL (2004) Structure of organoclays—an X-ray diffraction and thermogravimetric analysis study. J Colloid Interface Sci 277:116–120. https://doi.org/10.1016/j.jcis.2004.0.

Yotsuji K, Tachi Y, Sakuma H, Kawamura K (2021) Effect of interlayer cations on montmorillonite swelling: comparison between molecular dynamic simulations and experiments. Appl Clay Sci 204:106034. https://doi.org/10.1016/j.clay.2021.106034.

Zhang Z, Mat Yahaya F, Md Jaafar MF, Jing B, Feng J, Han K (2026) Application of activated river sediments and bentonite in supplementary cementitious materials (SCMs): a review. J Asian Archit Build Eng:1–26. https://doi.org/10.1080/13467581.2026.2689772.

Zhao C, Wang C, Hong H, Algeo TJ, Yin K, Ji K, Song B, Abels HA, Christidis GE (2021) Origin of dioctahedral smectites in lower Eocene Lulehe formation paleosols (Qaidam Basin, China). Appl Clay Sci 203:106026. https://doi.org/10.1016/j.clay.2021.106026.